REPORT NO.
UCB/SEMM-1999/06

STRUCTURAL ENGINEERING,
MECHANICS AND MATERIALS

ON THE FORMULATION OF HIGH-FREQUENCY DISSIPATIVE TIME-STEPPING ALGORITHMS FOR NONLINEAR DYNAMICS

PART II: SECOND ORDER METHODS

BY

F. ARMERO

AND

I. ROMERO

JULY 1999

DEPARTMENT OF CIVIL AND ENVIRONMENTAL ENGINEERING
UNIVERSITY OF CALIFORNIA
BERKELEY, CALIFORNIA

On the Formulation of High-Frequency Dissipative Time-Stepping Algorithms for Nonlinear Dynamics. Part II: Second Order Methods.*

by

F. ARMERO* & I. ROMERO

Structural Engineering, Mechanics and Materials
Department of Civil and Environmental Engineering
University of California, Berkeley CA 94720, USA

Abstract

We present in this paper the formulation of a new high-frequency dissipative time-stepping algorithm for nonlinear elastodynamics that is second order accurate in time. The new scheme exhibits unconditional energy dissipation and momentum conservation (and thus the given name of EDMC-2), leading also to the conservation of the relative equilibria of the underlying physical system. The unconditional character of these properties applies not only with respect to the time step size but, equally important, with respect to the considered elastic potential. Moreover, the dissipation properties are fully controlled through an algorithmic parameter, reducing to existing fully conserving schemes, if desired. The design of the new algorithm is described in detail, including a complete analysis of its dissipation/conservation properties in the fully nonlinear range of finite elasticity. To motivate the different constructions that lead to the dissipative properties of the final scheme, the same arguments are used first in the construction of new linear time-stepping algorithms for the system of linear elastodynamics, including first and second order schemes. The new schemes exhibit a rigorous decay of the physical energy, with the second order schemes formulated in a general two-stage formula accommodating the aforementioned control parameter in the dissipation of the energy. A complete spectral analysis of the new schemes is presented in this linear range to evaluate their different numerical properties. In particular, the dissipative character of the proposed schemes in the high-frequency range is fully demonstrated. In fact, it is shown that the new second order scheme is L-stable. Most remarkably, the extension of these ideas to the nonlinear range is accomplished avoiding the use of multi-stage formulas, given the freedom gained in using general nonlinear relations, while preserving the conservation laws of the momenta and the corresponding relative equilibria. Several representative numerical simulations are presented in the context of nonlinear elastodynamics to evaluate the performance of the newly proposed schemes.

KEY WORDS: nonlinear elastodynamics; time-stepping algorithms; high-frequency dissipation; relative equilibria; finite element method.

---

* Submitted to *Computer Methods in Applied Mechanics and Engineering.*

* Corresponding author (armero@ce.berkeley.edu).

1. Introduction

Typical problems in continuum and structural elastodynamics are characterized by a strong numerical stiffness, which motivates the use of implicit integrators for their temporal discretization. Many such time-stepping algorithms can be found in the literature; we refer to HUGHES [1987], among others, for a comprehensive account of many classical works in the linear range up to the mid 1980's. When developing these temporal schemes, the need of numerical dissipation in the high-frequency range, even though the underlying physical system may show full energy conservation, was soon realized if one is to arrive to robust implicit integrators. This feature is motivated, on one hand, by the need to eliminate the large modeling error accumulated in this range of frequencies, namely, the error introduced by spatial discretization of the infinite dimensional systems of interest. But more importantly, the large amount of work that can be found in this direction has been motivated by the need to avoid the numerical instabilities associated with the existence of a double unit root at infinite frequency in the amplification matrices of common conserving, mid-point type temporal approximations. In this way, the formulation of second-order schemes that exhibit these stability and dissipativity properties was an area of intensive research in the late 1970's to mid 1980's, and some of them have become standard in everyday practice; we refer again to HUGHES [1987] for details.

Despite this large amount of literature in the linear range, the development of similar schemes for the nonlinear finite deformation range is relatively recent. The need for additional developments along these lines is motivated by the fact that the aforementioned schemes, standard for applications involving linear elastodynamics, do lose their conservation/dissipation properties when applied to the nonlinear range, as illustrated in ARMERO & PETOCZ [1996], KUHL & CRISFIELD [1997] and ARMERO & ROMERO [1999] among others. The presence of numerical instabilities in nonlinear problems when employing schemes that are unconditionally stable in the linear range, including the aforementioned linearly dissipative schemes, has motivated the search for improved algorithms. Motivated by these remarks, the formulation of energy-momentum conserving schemes for nonlinear problems in continuum and structural elastodynamics has received a significant amount of attention recently. Representative references are SIMO & TARNOW [1992], CRISFIELD & SHI [1994] and GONZALEZ & SIMO [1995], among others. The proposed schemes consist basically of the mid-point rule algorithm, with a modified stress formula to assure energy conservation.

After these early experiences with energy conserving algorithms, the need of a controlled numerical dissipation in the high-frequency range to gain the robustness needed to solve the stiff problems of interest, as indicated above for the linear range, was also realized. Along these lines, we presented in ARMERO & PETOCZ [1996] some initial ideas on how to extend conserving schemes to incorporate energy dissipation in the context of dynamic contact problems. The proper modification of the stress formula (contact forces in contact problems) does lead to the incorporation of this numerical energy dissipation.

This and other approaches have been investigated further in KUHL & CRISFIELD [1997], CRISFIELD et al [1997] and KUHL & RAMM [1996,99] for nonlinear elastodynamics.

In ARMERO & ROMERO [1999], which we refer simply as Part I of this work hereafter, we have explored further the development of dissipative schemes in nonlinear dynamics. We formulated in this work a new time-stepping algorithm that is shown rigorously to exhibit unconditional energy dissipation while preserving the conservation laws of the linear and angular momentum in the mechanical problems of interest, the so-called energy-dissipative, momentum-conserving scheme (EDMC-1). Furthermore, it was shown in detail that the new algorithm does also preserve the relative equilibria of the underlying mechanical system, along the lines of the analysis presented in GONZALEZ & SIMO [1996] for the model problem of a nonlinear spring/mass system. More specifically, it was shown in Part I of this work that the newly proposed EDMC-1 dissipative scheme no only preserves these relative equilibria, characterized in the elastic systems under investigation by rigid motions superposed to a fixed deformation, but also lead to the introduction of the numerical dissipation in the high frequency range of the internal modes of the motion, with the solution tending asymptotically to the exact relative equilibria. This result was shown for two model problems (a simple nonlinear spring/mass system and a simplified model of thin beams), as well as for the general problem of nonlinear elastodynamics. In addition, a complete analysis was presented of the Newmark method (NEWMARK [1959]) and the HHT α-method (HILBER et al [1977]), as representative examples of the aforementioned linearly dissipative schemes, showing that these schemes not only lose their dissipative character, leading eventually to numerical instabilities, but also to the complete elimination of these relative equilibria of the system. The failure to preserve the conservation of angular momentum was shown to be the main drawback of these standard methods, in this respect. As a consequence, for the simple problem of a point mass rotating around a fixed point through a nonlinear elastic spring, the computed solution with these standard schemes either exploded for large time steps, or tended asymptotically to the static solution.

Despite the good stability and dissipation/conservation properties of the EDMC-1, this scheme is only first-order accurate in time. We present in this paper the formulation of a new time-stepping algorithm for nonlinear elastodynamics that exhibits the desired second-order accuracy in time while showing the same dissipation/conservation properties. Remarkably, the new scheme is based on the same structure as the EDMC-1 scheme, but with a more involved definition of the dissipation functions. For this reason, we simply refer to this new second-order scheme as the EDMC-2 scheme (energy-dissipative, momentum-conserving second-order scheme).

The development of high order dissipative schemes exhibiting numerical dissipation in the high-frequency range has been considered by several authors recently. For example, the formulation of such schemes for a model of elastic beams has been presented in BAUCHAU et al [1995], BAUCHAU & THERON [1996] and BOTASSO & BORRI [1998] and, more recently, in BAUCHAU & JOO [1999] for the continuum system of nonlinear elasto-

dynamics. However, these schemes do not show any control over the introduced numerical dissipation, in the form of an algorithmic parameter. In fact, these formulations are based on existing fixed multi-stage formulas, some of them arising from the application of the so-called discontinuous Galerkin in time (see e.g. JOHNSON et al [1984] and HUGHES & HULBERT [1988] for some of the original references), thus leading to a considerable added computational cost due to the doubling (extra displacement and velocity fields) for each additional stage considered in the numerical scheme. In some cases, the decay properties of the physical energy only applies to quadratic elastic potentials, especially if a second-order scheme is desired. In other cases, like in BAUCHAU & JOO [1999], no attention is given to the preservation of the conservation law of angular momentum which, as noted above, is a crucial property of the numerical scheme to capture fundamental qualitative properties of the underlying phase dynamics, even if numerical dissipation is introduced in the system.

In contrast, the EDMC schemes proposed in this work do show the numerical dissipation, as well as momenta conservation, with these properties holding independently of the elastic potential as well as the time step. In both the first and second order schemes an algorithmic parameter is introduced to control the numerical dissipation, recovering as a particular case a fully energy-conserving algorithm, if desired. Special care has been taken in the development of the second-order EDMC-2 presented in this work for nonlinear elastodynamics to avoid the cost associated to extra stages. Furthermore, the numerical dissipation is shown to be in the high-frequency range (an intrinsically linear concept) by deriving similar algorithms for linear elastodynamics following the same arguments, but without the constraint given by the conservation of the angular momentum (an intrinsically nonlinear concept).

In this context, before considering the problem of nonlinear elastodynamics in the second part of this paper, we consider first the development of time-stepping algorithms for linear elastodynamics that exhibit rigorously a decay of the physical energy of the system. We note that usually it is not the physical energy that decays along the solutions computed with classical dissipative schemes, but only a numerical norm of the discrete solution. Even though this is enough for the scheme to show numerical stability in the linear range, the dissipation of the actual energy of the physical system allows the extension of the linear scheme to the general nonlinear range, as the results in this work illustrate. In this way, we present first two new families of time-stepping algorithms for linear elastodynamics that show energy dissipation in the high-frequency range. We call the new schemes the energy-dissipative ED-1 and ED-2, for the first and second-order methods, respectively. A complete spectral analysis of these methods characterize their stability, dissipation and accuracy properties. In particular, the ED-2 scheme is shown to be L-stable (see e.g. HAIRER & WANNER [1991]), being formulated as a two-stage algorithm to maintain the linearity of the final formulas. Nonetheless, the freedom gained when extending the scheme to the nonlinear range (to the EDMC-2 scheme) allows to formulate the scheme with dissipation functions defined locally, without the need of introducing additional nodal

values of the displacements and velocities in a time step for a typical finite element solution of the problem of nonlinear elastodynamics. Furthermore, this extension is done in such a way that the conservation laws of linear and angular momenta, as well as the associated relative equilibria, are fully preserved.

An outline of the rest of the paper is as follows. Section 2 considers the problem of linear elastodynamics. After developing the new ED-1 and ED-2 schemes in Section 2.1.1 and 2.1.2, respectively, we present the spectral analysis of these methods in Section 2.2. The extension of these ideas to the nonlinear range is undertaken in Section 3, leading to the new EDMC-2 scheme, including rigorous proofs of the dissipation/conservation properties of the final time-stepping algorithm. The numerical implementation of the EDMC-2 scheme is described in detail in Appendix I. Section 4 includes several representative numerical simulations to evaluate the accuracy and dissipation/conservation properties of this scheme. Finally, some concluding remarks are drawn in Section 5.

2. The System of Linear Elastodynamics

We consider in this section the case of linear elastodynamics defined by the system of equations

$$\left.\begin{aligned} &\dot{\boldsymbol{d}} = \boldsymbol{v} \,, \\ &\boldsymbol{M}\dot{\boldsymbol{v}} = -\boldsymbol{K}\boldsymbol{d} + \boldsymbol{f}_{ext}(t) \,, \end{aligned}\right\} \tag{2.1}$$

for unknown functions in time $\boldsymbol{d}, \boldsymbol{v} : [0,T] \to \mathbb{R}^{n_{dof}}$, corresponding typically to a set of n_{dof} (nodal) displacements and velocities, respectively, with T denoting the time interval of interest. The symbol $\dot{(\cdot)}$ denotes the time derivative of the corresponding variable. We have made use in (2.1) of the classical notation of $\boldsymbol{M} \in \mathbb{R}^{n_{dof} \times n_{dof}}$ for the mass matrix, $\boldsymbol{K} \in \mathbb{R}^{n_{dof} \times n_{dof}}$ for the stiffness matrix, and $\boldsymbol{f}_{ext}(t) \in \mathbb{R}^{n_{dof}}$ for a general set of external forces. The classical properties of positive definiteness for the mass matrix $\boldsymbol{M}$ and positive semi-definiteness for the stiffness matrix $\boldsymbol{K}$ are assumed in this section, implying the relations

$$\boldsymbol{a} \cdot \boldsymbol{M}\boldsymbol{a} > 0 \qquad \text{and} \qquad \boldsymbol{a} \cdot \boldsymbol{K}\boldsymbol{a} \geq 0 \qquad \forall \boldsymbol{a} \in \mathbb{R}^{n_{dof}} \,, \quad \boldsymbol{a} \neq 0 \,, \tag{2.2}$$

where $\cdot$ denotes the standard Euclidean inner product in $\mathbb{R}^{n_{dof}}$ (i.e. $\boldsymbol{a} \cdot \boldsymbol{b} = a_i b_i$ summation implied among the n_{dof} components a_i and b_i of $\boldsymbol{a}$ and $\boldsymbol{b}$, respectively). The first-order system of ordinary differential equations (2.1) is accompanied with initial conditions

$$\boldsymbol{d}(0) = \bar{\boldsymbol{d}}_o \qquad \text{and} \qquad \boldsymbol{v}(0) = \bar{\boldsymbol{v}}_o \,, \tag{2.3}$$

for given initial values $\bar{\boldsymbol{d}}_o$ and $\bar{\boldsymbol{v}}_o$ of the displacements and velocities, respectively.

The system of equations (2.1) defines a linear Hamiltonian system. In this context, a standard calculation shows that

$$\dot{H} = \boldsymbol{f}_{ext} \cdot \boldsymbol{v} \,, \tag{2.4}$$

for the Hamiltonian function (the total energy)

$$H(\boldsymbol{d}, \boldsymbol{p}(\boldsymbol{v})) := \underbrace{\tfrac{1}{2}\, \boldsymbol{v} \cdot \boldsymbol{M}\boldsymbol{v}}_{\text{kinetic energy } K} + \underbrace{\tfrac{1}{2}\boldsymbol{d} \cdot \boldsymbol{K}\boldsymbol{d}}_{\text{potential energy } V} \,, \tag{2.5}$$

with the (linear) momenta $\boldsymbol{p}(\boldsymbol{v}) := \boldsymbol{M}\boldsymbol{v}$ (so the kinetic energy reads $K = \boldsymbol{p} \cdot \boldsymbol{M}^{-1}\boldsymbol{p}/2$) to follow the classical notation in the field. For the force-free case $\boldsymbol{f}_{ext} = 0$, we recover the classical conservation of energy relation

$$H(\boldsymbol{d}, \boldsymbol{p}(\boldsymbol{v})) = constant \,, \tag{2.6}$$

in time.

We are interested in time-stepping algorithms approximating the unknown functions $\boldsymbol{d}(t)$ and $\boldsymbol{v}(t)$ solutions of (2.1) through the sequence $\boldsymbol{d}_n \approx \boldsymbol{d}(t_n)$ and $\boldsymbol{v}_n \approx \boldsymbol{v}(t_n)$ ($n = 0, 1, 2, \ldots$) for a partition $[0, T] = \cup_n [t_n, t_{n+1}]$ of the time interval of interest and for given initial conditions $\boldsymbol{d}_o = \bar{\boldsymbol{d}}_o$ and $\boldsymbol{v}_o = \bar{\boldsymbol{v}}_o$ after (2.3). More specifically, it is the goal of this section to identify time-stepping algorithms that for a typical time step $[t_n, t_{n+1}]$ (with $\Delta t = t_{n+1} - t_n$, not necessarily constant in n) show the stability estimate

$$H_{n+1} - H_n = -\mathcal{D} \leq 0 \,, \tag{2.7}$$

for the homogeneous problem $\boldsymbol{f}_{ext} = 0$ and unconditionally in Δt, with $\mathcal{D} \geq 0$ defining the numerical dissipation. Here, $H_n := H(\boldsymbol{d}_n, \boldsymbol{p}(\boldsymbol{v}_n))$ for the the Hamiltonian $H(\cdot)$ in (2.5) of the continuum problem. We note that the estimate (2.7) is not a necessary condition for the numerical stability of a linear system like (2.1). The so-called energy method allows the identification of a general norm of the discrete solution satisfying a decaying estimate like (2.7), and not necessarily the physical (semi-)norm defined by the actual Hamiltonian; see e.g. HUGHES [1987], Chapter 9, for complete details. In fact, standard unconditionally stable time-stepping algorithms exhibiting a high-frequency dissipation, as it is the interest in this work (namely, the dissipative Newmark and the HHT schemes referred to in Section 1) do not satisfy the estimate (2.7). Instead an algorithmic norm (involving also contributions of the discrete acceleration approximating $\dot{\boldsymbol{v}}$) is shown to be decaying. In general, one can prove that for a spectrally stable scheme (that is, possessing a spectral radius less than one, as defined in Section 2.2 below) one can always construct, under some minor technical conditions, a numerical norm that decays in time; see HUGHES [1987], page 564. However, and as illustrated with the numerical examples presented in Part I of this work, these stability estimates in the linear problem do not extend to the nonlinear problem. The estimate (2.7), on the other hand, leads to a natural extension in the context of nonlinear dynamics as shown in the developments presented in this paper.

2.1. Some one-step dissipative schemes

With the stability estimate (2.7) in mind, we consider the general one-step method

$$\left.\begin{aligned} \frac{\boldsymbol{d}_{n+1}-\boldsymbol{d}_n}{\Delta t} &= \boldsymbol{g}_{cons}+\boldsymbol{g}_{diss}\ , \\ \boldsymbol{M}\frac{\boldsymbol{v}_{n+1}-\boldsymbol{v}_n}{\Delta t} &= -\left(\boldsymbol{f}_{cons}+\boldsymbol{f}_{diss}\right)+\tilde{\boldsymbol{f}}_{ext}\ , \end{aligned}\right\} \tag{2.8}$$

for an approximation $\tilde{\boldsymbol{f}}_{ext}$ of the external force vector (e.g. $\tilde{\boldsymbol{f}}_{ext}=\boldsymbol{f}_{ext}(t_{n+1/2})$). Here we have introduced conserving and dissipative approximations of the right-hand-side terms of the original equations (2.1), in the sense that the following equalities hold

$$\left.\begin{aligned} \boldsymbol{f}_{cons}\cdot\left(\boldsymbol{d}_{n+1}-\boldsymbol{d}_n\right) &= V_{n+1}-V_n\ , \\ \boldsymbol{g}_{cons}\cdot\boldsymbol{M}\left(\boldsymbol{v}_{n+1}-\boldsymbol{v}_n\right) &= K_{n+1}-K_n\ , \end{aligned}\right\} \tag{2.9}$$

and

$$\left.\begin{aligned} \boldsymbol{f}_{diss}\cdot\left(\boldsymbol{d}_{n+1}-\boldsymbol{d}_n\right) &= \mathcal{D}_V\ , \\ \boldsymbol{g}_{diss}\cdot\boldsymbol{M}\left(\boldsymbol{v}_{n+1}-\boldsymbol{v}_n\right) &= \mathcal{D}_K\ , \end{aligned}\right\} \tag{2.10}$$

as their counterparts in (2.1). The notation $V_n:=V(\boldsymbol{d}_n)$ and $K_n:=K(\boldsymbol{v}_n)$ for the exact potential $V(\cdot)$ and kinetic $K(\cdot)$ energies defined in (2.5) has been used in (2.9).

Multiplying $(2.8)_1$ by $\boldsymbol{M}(\boldsymbol{v}_{n+1}-\boldsymbol{v}_n)$, $(2.8)_2$ by $-(\boldsymbol{d}_{n+1}-\boldsymbol{d}_n)$ and adding the resulting expressions, we obtain

$$\underbrace{\left(K_{n+1}+V_{n+1}\right)}_{H_{n+1}}-\underbrace{\left(K_n+V_n\right)}_{H_n}=-\underbrace{\mathcal{D}_K+\mathcal{D}_V}_{\mathcal{D}}\ , \tag{2.11}$$

identifying the numerical dissipation $\mathcal{D}$ in (2.7) with $\mathcal{D}=\mathcal{D}_V+\mathcal{D}_K$ in this case. We emphasize again the need of a non-negative dissipation $\mathcal{D}\geq 0$ for numerical stability, not necessarily each of its components $\mathcal{D}_K$ and $\mathcal{D}_V$. Similarly, we reiterate our interest that the final numerical dissipation $\mathcal{D}$ is controllable and in the high-frequency range, as motivated in the introduction presented in Section 1.

In this linear setting, linear conservative terms are easily obtained through the second-order mid-point approximations

$$\boldsymbol{f}_{cons}=\tfrac{1}{2}\boldsymbol{K}\left(\boldsymbol{d}_{n+1}+\boldsymbol{d}_n\right)=:\boldsymbol{K}\boldsymbol{d}_{n+\frac{1}{2}}\ ,\qquad\text{and}\qquad \boldsymbol{g}_{cons}=\tfrac{1}{2}\left(\boldsymbol{v}_{n+1}+\boldsymbol{v}_n\right)=:\boldsymbol{v}_{n+\frac{1}{2}}\ . \tag{2.12}$$

The estimates (2.9) can be easily verified. Therefore, the discrete system (2.8) defines in this case a consistent approximation of (2.1) if

$$\boldsymbol{f}_{diss}\sim\mathcal{O}(\Delta t^p)\quad\text{and}\quad \boldsymbol{g}_{diss}\sim\mathcal{O}(\Delta t^p)\quad\text{for}\quad p\geq 1\ , \tag{2.13}$$

where we have used the standard notation of $\mathcal{O}(\cdot)$ for the "big-oh" (that is, $\lim \mathcal{O}(x^p)/x^{(p-1)} \to 0$ as $x \to 0$). Since in the resulting consistent approximations the differences

$$\boldsymbol{d}_{n+1} - \boldsymbol{d}_n \sim \mathcal{O}(\Delta t) \qquad \text{and} \qquad \boldsymbol{v}_{n+1} - \boldsymbol{v}_n \sim \mathcal{O}(\Delta t) \,, \tag{2.14}$$

we conclude from (2.10) that (2.13) implies that $\mathcal{D}_V, \mathcal{D}_K \sim \mathcal{O}(\Delta t^{p+1})$. The final numerical scheme will exhibit an order of accuracy of at least $\min\{2, p\}$, that is, first or second order methods. We consider in the next two sections these two cases separately.

Remark 2.1. We have considered, for simplicity in the exposition, the Hamiltonian case given by the system of equations (2.1). The consideration of linear damping in $(2.1)_2$, that is,

$$\boldsymbol{M}\dot{\boldsymbol{v}} = -\boldsymbol{C}\boldsymbol{v} - \boldsymbol{K}\boldsymbol{d} + \boldsymbol{f}_{ext} \,, \tag{2.15}$$

for a positive semi-definite damping matrix $\boldsymbol{C}$ can be easily incorporated in the developments of this section. In particular, the general approximation of the damping term

$$\boldsymbol{C}\boldsymbol{v} \to \boldsymbol{C}(\boldsymbol{d}_{n+1} - \boldsymbol{d}_n)/\Delta t \,, \tag{2.16}$$

leads to a dissipative approximation, with the added physical dissipation $\mathcal{D}_C = (\boldsymbol{d}_{n+1} - \boldsymbol{d}_n) \cdot \boldsymbol{C}(\boldsymbol{d}_{n+1} - \boldsymbol{d}_n)/\Delta t \geq 0$ to the numerical dissipation $\mathcal{D}$ in (2.11). We note, however, that the consideration of an artificial damping $\boldsymbol{C}$ alone, not necessarily modeling a physical damping, does not lead to the introduction of dissipation in the high-frequency range (see e.g. HUGHES [1983], page 97). □

2.1.1. First–order dissipative schemes (ED-1)

Given the definiteness properties (2.2) of the mass and stiffness matrices, the simplest choice of dissipative terms $\boldsymbol{f}_{diss}$ and $\boldsymbol{g}_{diss}$ satisfying the dissipation estimate (2.7) is given by

$$\boldsymbol{f}_{diss} = \chi_1 \tfrac{1}{2} \boldsymbol{K} (\boldsymbol{d}_{n+1} - \boldsymbol{d}_n) \,, \qquad \text{and} \qquad \boldsymbol{g}_{diss} = \chi_2 \tfrac{1}{2} (\boldsymbol{v}_{n+1} - \boldsymbol{v}_n) \,. \tag{2.17}$$

in terms of two numerical parameters χ_1 and χ_2. With these definitions, the relations (2.8) lead to the quadratic dissipation functions

$$\left.\begin{aligned} \mathcal{D}_V &= \chi_1 \tfrac{1}{2} (\boldsymbol{d}_{n+1} - \boldsymbol{d}_n) \cdot \boldsymbol{K} (\boldsymbol{d}_{n+1} - \boldsymbol{d}_n) \geq 0 \,, \\ \mathcal{D}_K &= \chi_2 \tfrac{1}{2} (\boldsymbol{v}_{n+1} - \boldsymbol{v}_n) \cdot \boldsymbol{M} (\boldsymbol{v}_{n+1} - \boldsymbol{v}_n) \geq 0 \,, \end{aligned}\right\} \tag{2.18}$$

for $\chi_1, \chi_2 \geq 0$ by (2.2). Given (2.14), we conclude that the choices determined by the relations (2.17) define a first-order scheme (note that $\mathcal{D}_V, \mathcal{D}_K \sim \mathcal{O}(\Delta t^2)$). The resulting scheme is denoted ED-1 (energy dissipative, first order), and reduces to the scheme referred to as $\theta-$method in WOOD [1990] for the particular case given by $\chi_1 = \chi_2$.

2.1.2. Second–order dissipative schemes (ED-2)

We observe that the limited first-order character of the approximations (2.17) arises from the first-order differences (2.14). Therefore, to arrive to second-order dissipative linear schemes, we consider the alternative expressions for the dissipative terms

$$\boldsymbol{f}_{diss} = \tfrac{1}{2}\, \boldsymbol{K}(\tilde{\boldsymbol{d}}_n - \boldsymbol{d}_n)\,, \qquad \text{and} \qquad \boldsymbol{g}_{diss} = \tfrac{1}{2}\, (\tilde{\boldsymbol{v}}_n - \boldsymbol{v}_n)\,, \tag{2.19}$$

for intermediate stage values $\tilde{\boldsymbol{d}}_n$ and $\tilde{\boldsymbol{v}}_n$. We are interested in these intermediate values defining a second-order approximation of the corresponding values at t_n, that is,

$$\tilde{\boldsymbol{d}}_n - \boldsymbol{d}_n \sim \mathcal{O}(\Delta t^2) \qquad \text{and} \qquad \tilde{\boldsymbol{v}}_n - \boldsymbol{v}_n \sim \mathcal{O}(\Delta t^2)\,, \tag{2.20}$$

so $\boldsymbol{f}_{diss}$ and $\boldsymbol{g}_{diss}$ are second-order $\mathcal{O}(\Delta t^2)$ in Δt. This order can be achieved with the relations

$$\left.\begin{aligned} \tilde{\boldsymbol{d}}_n &= \boldsymbol{d}_n \quad + \Delta t\ \alpha\ (\tilde{\boldsymbol{v}}_n - \boldsymbol{v}_{n+1})\,, \\ \boldsymbol{M}\tilde{\boldsymbol{v}}_n &= \boldsymbol{M}\boldsymbol{v}_n - \Delta t\ \alpha\ \boldsymbol{K}(\tilde{\boldsymbol{d}}_n - \boldsymbol{d}_{n+1}) \quad [+\Delta t\ \hat{\boldsymbol{f}}_{ext}]\,, \end{aligned}\right\} \tag{2.21}$$

for an algorithmic parameter α. The term $[+\Delta t\ \hat{\boldsymbol{f}}_{ext}]$ in $(2.21)_2$ has been added to recover some existing methods as particular cases. For the methods proposed in this paper, we simply take $\hat{\boldsymbol{f}}_{ext} \equiv 0$. We note that the second-order relations (2.20) are automatically satisfied for the definitions (2.21), even for $\hat{\boldsymbol{f}}_{ext} = 0$. More generally, we would need $\hat{\boldsymbol{f}}_{ext} \sim \mathcal{O}(\Delta t)$.

The particular cross definitions (2.21) for the intermediate values $\tilde{\boldsymbol{d}}_n$ and $\tilde{\boldsymbol{v}}_n$ have been introduced to arrive at dissipative approximations for any value of the parameter α. Indeed, combining equations (2.19) and (2.21), the numerical dissipation $\mathcal{D}$ is given by (2.10) for $\alpha \neq 0$ as

$$\begin{aligned} \mathcal{D} = \mathcal{D}_V + \mathcal{D}_K &= \boldsymbol{g}_{diss} \cdot \boldsymbol{M}\,(\boldsymbol{v}_{n+1} - \boldsymbol{v}_n)\ + \boldsymbol{f}_{diss} \cdot (\boldsymbol{d}_{n+1} - \boldsymbol{d}_n) \\ &= \tfrac{1}{2}\,(\tilde{\boldsymbol{v}}_n - \boldsymbol{v}_n) \cdot \boldsymbol{M}(\boldsymbol{v}_{n+1} - \boldsymbol{v}_n) + \tfrac{1}{2}\,(\tilde{\boldsymbol{d}}_n - \boldsymbol{d}_n) \cdot \boldsymbol{K}(\boldsymbol{d}_{n+1} - \boldsymbol{d}_n) \\ &= \tfrac{1}{2}\,(\tilde{\boldsymbol{v}}_n - \boldsymbol{v}_n) \cdot \boldsymbol{M}(\tilde{\boldsymbol{v}}_n - \boldsymbol{v}_n) + \tfrac{1}{2}\,(\tilde{\boldsymbol{d}}_n - \boldsymbol{d}_n) \cdot \boldsymbol{K}(\tilde{\boldsymbol{d}}_n - \boldsymbol{d}_n) \\ &\quad + \tfrac{1}{2}\,(\tilde{\boldsymbol{v}}_n - \boldsymbol{v}_n) \cdot \boldsymbol{M}(\boldsymbol{v}_{n+1} - \tilde{\boldsymbol{v}}_n) + \tfrac{1}{2}\,(\tilde{\boldsymbol{d}}_n - \boldsymbol{d}_n) \cdot \boldsymbol{K}(\boldsymbol{d}_{n+1} - \tilde{\boldsymbol{d}}_n) \\ &= \tfrac{1}{2}\,(\tilde{\boldsymbol{v}}_n - \boldsymbol{v}_n) \cdot \boldsymbol{M}(\tilde{\boldsymbol{v}}_n - \boldsymbol{v}_n) + \tfrac{1}{2}\,(\tilde{\boldsymbol{d}}_n - \boldsymbol{d}_n) \cdot \boldsymbol{K}(\tilde{\boldsymbol{d}}_n - \boldsymbol{d}_n) \\ &\quad - \tfrac{1}{2}\,\frac{1}{\Delta t\alpha}(\tilde{\boldsymbol{v}}_n - \boldsymbol{v}_n) \cdot \boldsymbol{M}(\tilde{\boldsymbol{d}}_n - \boldsymbol{d}_n) + \tfrac{1}{2}\,\frac{1}{\Delta t\alpha}\boldsymbol{M}(\tilde{\boldsymbol{d}}_n - \boldsymbol{d}_n) \cdot (\tilde{\boldsymbol{v}}_n - \boldsymbol{v}_n) \\ &= \tfrac{1}{2}\,(\tilde{\boldsymbol{v}}_n - \boldsymbol{v}_n) \cdot \boldsymbol{M}(\tilde{\boldsymbol{v}}_n - \boldsymbol{v}_n) + \tfrac{1}{2}\,(\tilde{\boldsymbol{d}}_n - \boldsymbol{d}_n) \cdot \boldsymbol{K}(\tilde{\boldsymbol{d}}_n - \boldsymbol{d}_n) \geq 0\,, \end{aligned} \tag{2.22}$$

given the assumed positive definiteness properties (2.2). For the case $\alpha = 0$, the estimate (2.22) still holds since in this case we have from (2.21) $\tilde{\boldsymbol{d}}_n = \boldsymbol{d}_n$ and $\tilde{\boldsymbol{v}}_n = \boldsymbol{v}_n$, so $\boldsymbol{f}_{diss} = 0$,

$\boldsymbol{g}_{diss} = 0$, and $\mathcal{D} = \mathcal{D}_V = \mathcal{D}_K = 0$, recovering the conserving scheme. We note that, in contrast we the first-order methods introduced in Section 2.1.1, it is the total dissipation $\mathcal{D}$ (and not necessarily each component $\mathcal{D}_V$ and $\mathcal{D}_K$) that is non-negative, as needed, for the second-order schemes defined by (2.19). The cross definitions (2.21) of $\tilde{\boldsymbol{d}}_n$ and $\tilde{\boldsymbol{v}}_n$ allow the cancellation of terms in the proof of the estimate (2.22) resulting in the dissipative character of the final scheme.

We can recognize several existing algorithms as particular cases of the time-stepping algorithms given by (2.19) and (2.21). Namely, we have:

i. $\alpha = 0$ leads to the trapezoidal rule (with $\hat{\boldsymbol{f}}_{ext} = 0$), the conserving formula (2.12).

ii. $\alpha = 1/6$ leads to (linear in time) discontinuous Galerkin for

$$\tilde{\boldsymbol{f}}_{ext} = \frac{1}{\Delta t} \int_{t_n}^{t_{n+1}} \boldsymbol{f}_{ext}(t)\, dt\,, \tag{2.23}$$

in the original discrete approximation (2.8), and

$$\hat{\boldsymbol{f}}_{ext} = \int_{t_n}^{t_{n+1}} \frac{t_{n+1/2} - t}{2\Delta t^2} \boldsymbol{f}_{ext}(t)\, dt\,. \tag{2.24}$$

in (2.21). These very particular choices lead to a third-order scheme; see JOHNSON et al [1984].

iii. $\alpha = 1/2$ leads to the Lobatto IIIC Runge-Kutta method for

$$\tilde{\boldsymbol{f}}_{ext} = \tfrac{1}{2}\Big(\boldsymbol{f}_{ext}(t_n) + \boldsymbol{f}_{ext}(t_{n+1})\Big)\,, \tag{2.25}$$

in the original discrete approximation (2.8), and

$$\hat{\boldsymbol{f}}_{ext} = \tfrac{1}{2}\Big(\boldsymbol{f}_{ext}(t_n) - \boldsymbol{f}_{ext}(t_{n+1})\Big)\,, \tag{2.26}$$

in (2.21).

Hence, the new methods (2.19)-(2.21) can be seen to be extensions of the particular cases indicated above, with the algorithmic parameter α controlling the introduced numerical dissipation. The dissipative estimate (2.22) shows the unconditional stability of all the resulting schemes, that is, for any α. The spectral analysis presented in the following section shows that numerical energy dissipation in the high-frequency range is accomplished for $\alpha > 0$.

Remarks 2.2.

1. We note the computational expense added by the introduction of the intermediate stage (2.21), leading to an algebraic system of equations in $4 \cdot n_{dof}$ unknowns ($\boldsymbol{d}_{n+1}$, $\boldsymbol{v}_{n+1}$, $\tilde{\boldsymbol{d}}_n$ and $\tilde{\boldsymbol{v}}_n$), typical of multi-stage implementations. The cross character of the relations (2.21) leads to a fully coupled system of equations in this $4 \cdot n_{dof}$ unknowns, and its solution does not reduce to the simple evaluation of two dynamic stages. For this reason, the use of the proposed numerical schemes in the linear setting considered in this section may appear rather limited in front of existing single stage formulas. However, and as shown in Section 3, the algorithms described in this section provide the basis for the formulation of dissipative time-stepping algorithms in the fully nonlinear range. In addition, the generality added by the consideration of nonlinear formulae allows to these costly multi-stage implementations and preserve other fundamental properties of the nonlinear dynamics.

2. We observe that the use of other mass and stiffness matrices in equations (2.19) and $(2.21)_2$, say $\hat{\boldsymbol{M}}$ and $\hat{\boldsymbol{K}}$, would have led to the same energy decay estimate (2.22), as long as these matrices satisfy the conditions (2.2). This observation also applies to the relations (2.17) and (2.18) for the ED-1 scheme. This arbitrariness corresponds, in essence, to a scaling of the algorithmic parameters, α or χ_1 and χ_2, respectively. □

2.2. Spectral analysis

The complete characterization of the stability and accuracy properties of time-stepping algorithms in the linear range can be obtained through a spectral analysis of the discrete equations. In particular, and following standard arguments (see e.g. HUGHES [1987], Chapter 9, for complete details), we consider the homogeneous system of equations

$$\left.\begin{aligned} \dot{d} &= v \,, \\ \dot{v} &= -\omega^2 \, d \,, \end{aligned}\right\} \quad \Longleftrightarrow \quad \ddot{d} + \omega^2 \, d = 0 \,, \tag{2.27}$$

corresponding to a free one-degree of freedom linear oscillator of natural frequency ω. The system equations (2.27) can be understood as governing one of the modal equations of the multi-dimensional system (2.1), for the corresponding frequency ω of the response. Indeed, and as a classical argument shows, if we denote by $\boldsymbol{\nu}_i$ and ω_i the eigenvectors and eigenvalues of the generalized eigenproblem

$$\boldsymbol{K}\boldsymbol{\nu}_i = \omega_i^2 \, \boldsymbol{M}\boldsymbol{\nu}_i \,, \quad \text{for} \quad i = 1, n_{dof} \,, \tag{2.28}$$

(no sum in i implied), the contraction of the equations (2.1) with each eigenvector ν_i leads to the scalar equations (2.27) for each modal component $d_i := \boldsymbol{\nu}_i \cdot \boldsymbol{d}$ and $v_i := \boldsymbol{\nu}_i \cdot \boldsymbol{v}$ (sub-indices i having been omitted in (2.27)).

Following the same modal projection argument, the general class of linear time-stepping algorithms (2.8), with (2.17) or (2.19), leads to the same discrete relations when applied directly to the scalar system (2.27). For a typical time increment $[t_n, t_{n+1}]$ (with $\Delta t = t_{n+1} - t_n$), the resulting equations can be written as

$$\left\{ \begin{array}{c} d_{n+1} \\ \Delta t v_{n+1} \end{array} \right\} = \boldsymbol{A}(\Omega) \left\{ \begin{array}{c} d_n \\ \Delta t v_n \end{array} \right\} , \tag{2.29}$$

for the algorithmic amplification matrix $\boldsymbol{A}(\Omega) \in \mathbb{R}^{2\times 2}$, function of the (non-dimensional) sampling frequency $\Omega := \omega\, \Delta t \in [0, \infty)$.

The interest is focused on the properties of the eigenvalues $\gamma_i \in \mathbb{C}$ $(i = 1, 2)$ of the amplification matrix $\boldsymbol{A}(\Omega)$, with the spectral radius $\rho(\Omega)$ for the frequency Ω defined as

$$\rho(\Omega) := \max_{i=1,2} |\gamma_i(\Omega)| \quad \text{with} \quad \rho_\infty := \lim_{\Omega\to\infty} \rho(\Omega) . \tag{2.30}$$

The spectral stability of the numerical scheme is then defined by $\rho(\Omega) \leq 1$, with linearly independent eigenvectors for repeated eigenvalues γ_i (otherwise, if the eigenvectors of repeated eigenvalues are linearly dependent, $\rho(\Omega) < 1$ strictly). In particular, the numerical dissipation in the high-frequency range is reflected by the property $\rho_\infty < 1$, strictly. A complete characterization of the spectral properties of the numerical scheme is obtained by considering the standard spectral error measures: the relative frequency error

$$e_\Omega := \frac{\Omega_d - \Omega}{\Omega} \quad \text{where} \quad \Omega_d = |\mathrm{Im}(\ln \gamma_i)| ,$$

(note that γ_1 and γ_2 are real or complex conjugate, so $|\mathrm{Im}(\gamma_1)| = |\mathrm{Im}(\gamma_2)|$), and the algorithmic damping ratio

$$\xi_d := \min_{i=1,2} \xi_{d_i} \quad \text{where} \quad \xi_{d_i} := -\frac{1}{\Omega_d} \mathrm{Re}(\ln \gamma_i) \quad \text{for} \quad i = 1, 2 . \tag{2.31}$$

We refer again to HUGHES [1987], Chapter 9, for complete details on these classical concepts.

i. *First-order ED-1 schemes.* The amplification matrix (2.29) for the ED-1 scheme (2.17) is given by

$$^{ED1}\boldsymbol{A}(\Omega) = \begin{bmatrix} 1 & -\beta_2^+ \\ \Omega^2\, \beta_1^+ & 1 \end{bmatrix}^{-1} \begin{bmatrix} 1 & \beta_2^- \\ -\Omega^2\, \beta_1^- & 1 \end{bmatrix} = \frac{1}{\Delta} \begin{bmatrix} 1 - \Omega^2 \beta_1^+ \beta_2^- & 1 \\ -\Omega^2 & 1 - \Omega^2 \beta_1^- \beta_2^+ \end{bmatrix} , \tag{2.32}$$

where

$$\left. \begin{array}{ll} \beta_1^+ := \frac{1}{2}(1 + \chi_1) , & \beta_1^- := \frac{1}{2}(1 - \chi_1) \\ \beta_2^+ := \frac{1}{2}(1 + \chi_2) & \beta_2^- := \frac{1}{2}(1 - \chi_2) \end{array} \right\} \quad \text{and} \quad \Delta := 1 + \Omega^2 \beta_1^+ \beta_2^+ , \tag{2.33}$$

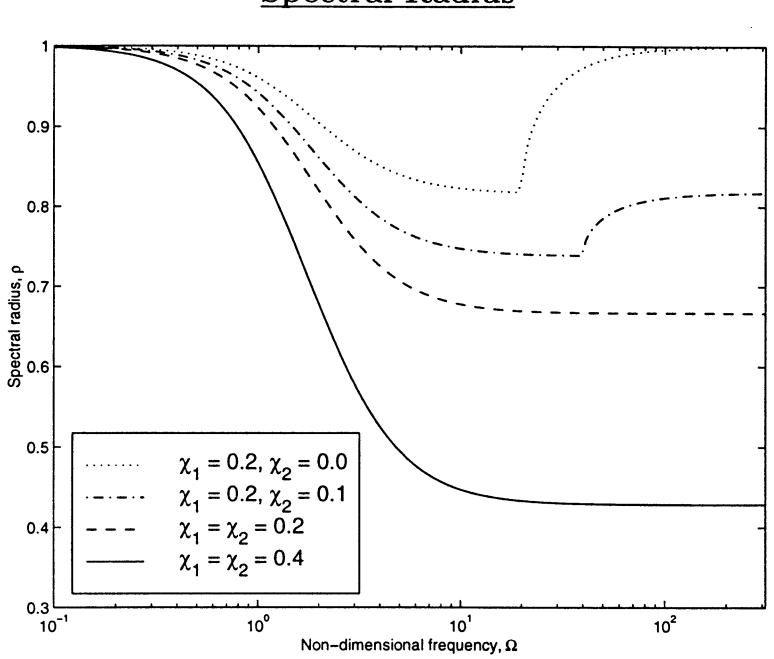

FIGURE 2.1. Spectral analysis, ED-1 schemes. Distribution of the spectral radius $\rho(\Omega)$ in terms of the sampling frequency $\Omega = \omega\Delta t$ of a linear oscillator for different numerical parameters χ_1 and χ_2. Note that $\rho_\infty = \max_{i=1,2}(|1-\chi_i|/1+\chi_i)$.

in terms of the algorithmic parameters χ_1 and χ_2. The eigenvalues of the amplification matrix (2.32) are given in closed-form by

$$^{ED1}\gamma_{1,2} = \frac{1}{\Delta}\left(1 - \frac{\Omega^2}{2}\left(\beta_1^+\beta_2^- + \beta_1^-\beta_2^+\right) \pm \Omega\sqrt{\frac{\Omega^2}{4}\left(\beta_1^+\beta_2^+ - \beta_1^-\beta_2^-\right)^2 - 1}\right) . \quad (2.34)$$

Some analysis shows that $\rho(\Omega) \leq 1$ for $\chi_1, \chi_2 \geq 0$, and leads to the closed-form expression

$$\boxed{^{ED1}\rho_\infty = \max\left\{\frac{|1-\chi_1|}{1+\chi_1}, \frac{|1-\chi_2|}{1+\chi_2}\right\},} \quad (2.35)$$

for the spectral radius at infinity. We observe that $\rho_\infty < 1$ if $\chi_1 > 0$ and $\chi_2 > 0$, thus requiring the presence of dissipative terms in both equations (2.8) for this class of first-order schemes to exhibit high-frequency numerical dissipation.

The expression (2.34) shows that a bifurcation from two complex conjugate to two real eigenvalues occurs for the sample frequency

$$\Omega_{bif} = \frac{2}{\left|\beta_1^-\beta_2^+ - \beta_1^+\beta_2^-\right|} , \quad (2.36)$$

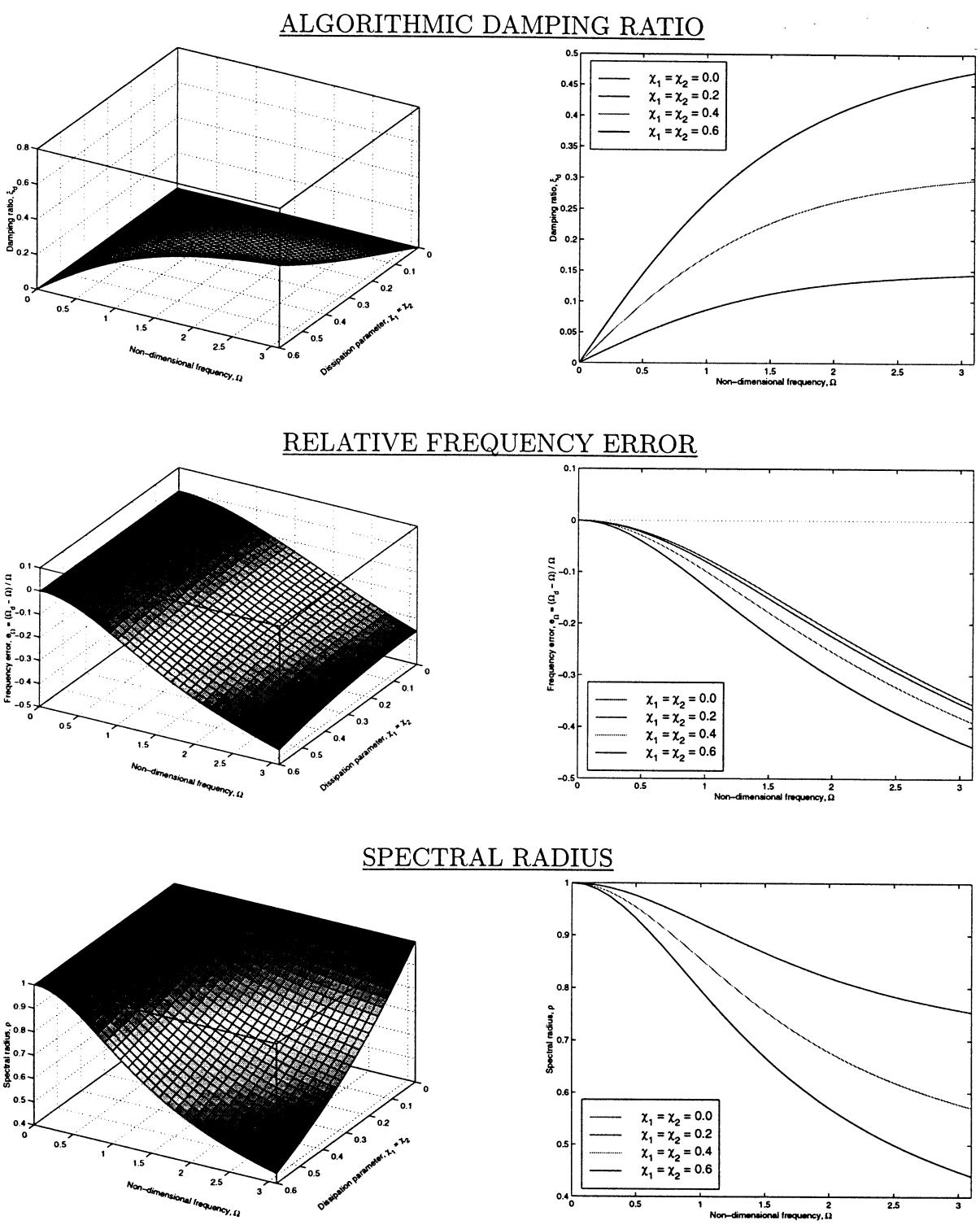

FIGURE 2.2. Spectral analysis, ED-1 schemes. Distribution of the algorithmic damping ratio $\xi_d(\Omega)$, relative frequency error $e_\Omega(\Omega)$ and spectral radius $\rho(\Omega)$ in terms of the sampling frequency $\Omega = \omega\Delta t$ of a linear oscillator and the numerical parameter χ $(= \chi_1 = \chi_2)$.

at which a repeated real eigenvalue exists. The closed-form expression (2.34) reveals that in this case $\rho(\Omega_{bif}) < 1$, strictly. We also observe that $\Omega_{bif} = \infty$ if and only if $\chi_1 = \chi_2$. This bifurcation can be seen in Figure 2.1 to reduce the spectral radius at Ω_{bif} whenever $\chi_1 \neq \chi_2$. From these considerations (or directly from the expression (2.35) of the spectral radius at infinity), we conclude the optimality of the choice $\chi_1 = \chi_2$.

Figure 2.2 depicts the distribution of the algorithmic damping ratio $\xi_d(\Omega)$, relative frequency error $e_\Omega(\Omega)$ and spectral radius $\rho(\Omega)$ for this case. The three-dimensional plots in the left column show these values versus the sampling frequency Ω and the algorithmic parameter $\chi_1 = \chi_2$. The 2-D plots in the right column correspond to sections of these 3D plots for a different fixed algorithmic parameter. The absence of numerical dissipation (reflected by the values $\xi_d(\Omega) \equiv 0$ or $\rho(\Omega) = 1$) in the conservative case $\chi_1 = \chi_2 = 0$ is apparent, with increasing values of this numerical dissipation for increasing values of the algorithmic parameter $\chi_1 = \chi_2$. The relative frequency error e_Ω is observed to be non-positive, thus concluding that the computed frequencies Ω_d are smaller than the exact frequency Ω for this scheme. Alternatively, we may say that the computed periods ($T_d := \Delta t\ 2\pi/\Omega_d$) are always elongated when compared with the exact periods ($T := \Delta t\ 2\pi/\Omega$).

A calculation based on (2.34) results in the asymptotic values

$$\xi_d(\Omega) = \frac{\chi}{2}\Omega + \mathcal{O}(\Omega^2)\,, \tag{2.37}$$

$$e_\Omega(\Omega) = -\frac{1}{4}\left(\chi^2 + \frac{1}{3}\right)\Omega^2 + \mathcal{O}(\Omega^3)\,, \tag{2.38}$$

as $\Omega \to 0$, and where the optimal case $\chi_1 = \chi_2 = \chi$ has been assumed. The first-order accuracy of the method (unless $\chi = 0$, that is, the conservative case) is a consequence of the first-order nature of the algorithmic damping ratio $\xi_d(\Omega)$ in (2.37). Note that the dissipation function $\mathcal{D} := \mathcal{D}_V + \mathcal{D}_K$ in (2.18) is of second order in Δt, but the final scheme is first-order only, as discussed during the design of the algorithm in Section 2.1.1. This first-order accuracy of the scheme is reflected in Figure 2.2 by the non-zero slope at $\Omega = 0$ of the distribution of the algorithmic damping ratio $\xi_d(\Omega)$ for a fixed algorithmic parameter $\chi_1 = \chi_2$, in accordance with (2.37).

ii. *Second-order ED-2 schemes.* The amplification matrix (2.29) for the ED-2 scheme (2.19) is given by

$$^{ED2}\boldsymbol{A}(\Omega) = \left(\boldsymbol{A}_1 - \boldsymbol{A}_2\boldsymbol{A}_3^{-1}\boldsymbol{A}_4\right)^{-1}\left(\mathbf{1} - \boldsymbol{A}_2\boldsymbol{A}_3^{-1}\right)\,, \tag{2.39}$$

where

$$\boldsymbol{A}_1 = \begin{bmatrix} 1 & -\frac{1}{2} \\ \frac{\Omega^2}{2} & 1 \end{bmatrix}\,,\quad \boldsymbol{A}_2 = \begin{bmatrix} 0 & -\frac{1}{2} \\ \frac{\Omega^2}{2} & 0 \end{bmatrix}\,,\quad \boldsymbol{A}_3 = \begin{bmatrix} 1 & -\alpha \\ \Omega^2\alpha & 1 \end{bmatrix}\,,\quad \boldsymbol{A}_4 = \begin{bmatrix} 0 & \alpha \\ -\Omega^2\alpha & 0 \end{bmatrix}\,, \tag{2.40}$$

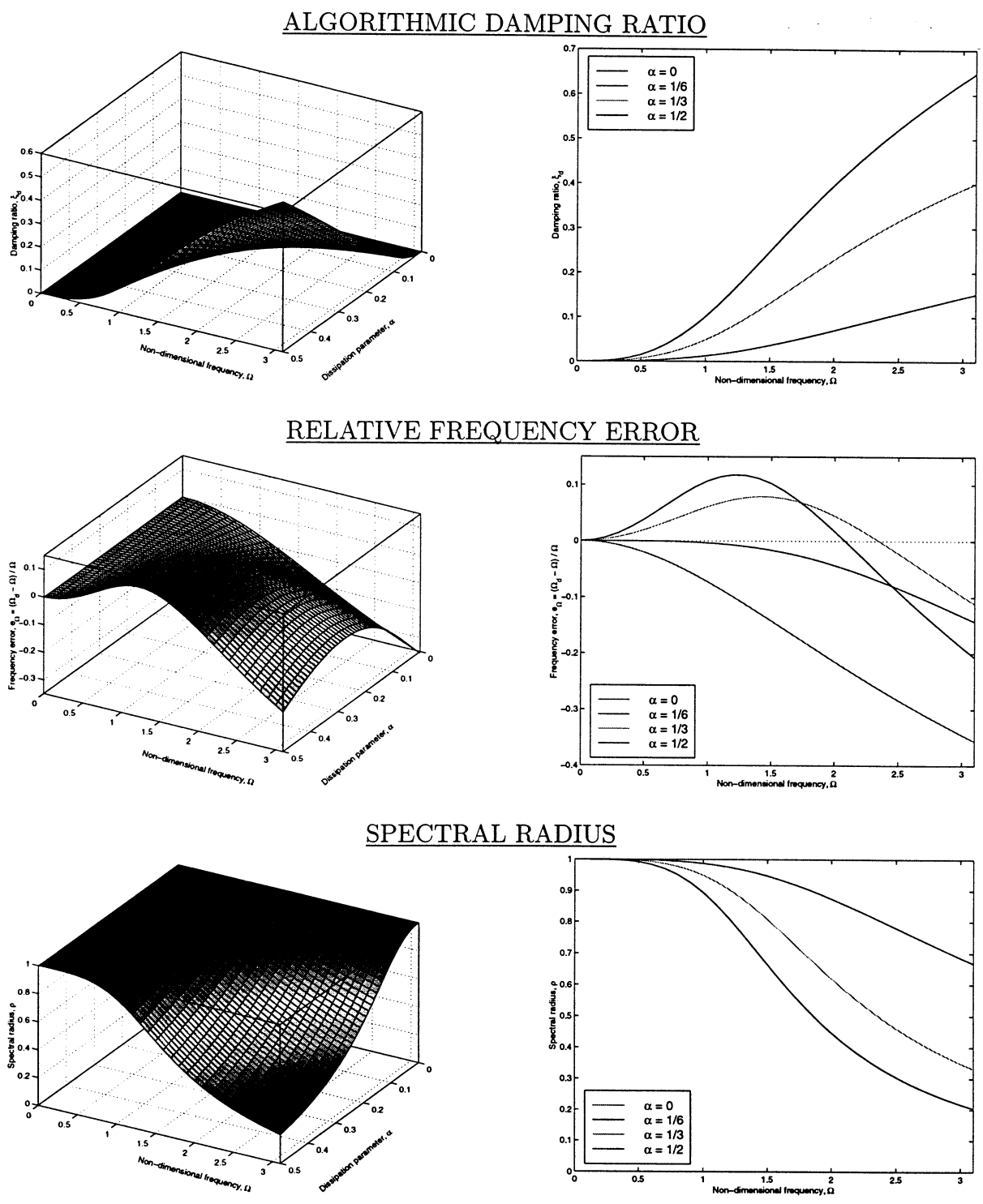

FIGURE 2.3. Spectral analysis, ED-2 schemes. Distribution of the algorithmic damping ratio $\xi_d(\Omega)$, relative frequency error $e_d(\Omega)$ and spectral radius $\rho(\Omega)$ in terms of the sampling frequency $\Omega = \omega\Delta t$ of a linear oscillator and the numerical parameter α. Note that $\rho_\infty = 0$ and the second-order accuracy in time (as reflected by the zero slope at $\Omega = 0$).

in terms of the algorithmic parameter α. After a long but straightforward calculation, the eigenvalues of the amplification matrix (2.40) are given in closed-form as

$$^{ED2}\gamma_{1,2} = \frac{1 - \frac{\Omega^2}{4} - \alpha\,\Omega^2 + \alpha^2\,\Omega^2 \pm i\,\Omega\,\left|1 - \alpha\frac{\Omega^2}{2} + \alpha^2\,\Omega^2\right|}{1 + \frac{\Omega^2}{4} - \alpha\,\Omega^2 + \alpha^2\,\Omega^2 + \alpha^2\,\Omega^4}\,, \tag{2.41}$$

where $i = \sqrt{-1}$. The spectral radius is then given by the closed-form expression (for $\alpha > 0$)

$$^{ED2}\rho(\Omega) = \max_{i,2}|\gamma_i(\Omega)| = \sqrt{1 - \frac{\alpha^2\,\Omega^4}{1 + \frac{\Omega^2}{4} - \alpha\,\Omega^2 + \alpha^2\,\Omega^2 + \alpha^2\,\Omega^4}}\,, \tag{2.42}$$

which reduces to $\rho(\Omega) \equiv 1$ for the conservative case $\alpha = 0$ (no dissipation in this case for any sampling frequency Ω) and for $\alpha < 0$.

From (2.41) and (2.42), we can also observe the limit

$$\lim_{\Omega\to\infty} {}^{ED2}\gamma_{1,2} = 0\,, \quad \text{so} \quad \boxed{{}^{ED2}\rho_\infty = 0\,,} \tag{2.43}$$

for $\alpha > 0$, thus showing a full numerical dissipation in the infinite frequency. The ED-2 schemes are then *L-stable* for $\alpha > 0$ (see e.g. HAIRER & WANNER [1991]). We note that, even though a control over the spectral radius at infinity ρ_∞ may certainly be a desired feature (for example, for the calibration of the algorithmic parameter α), the infinite sampling frequency may be considered as "far away as needed" in many practical applications. With this we mean that we still have full control over the range of finite frequencies for a particular problem and its discretization (in the sense that the desired amount of damping can be introduced through the variation of the algorithmic parameter α), while still exhibiting energy dissipation in the infinite (say larger or unresolved) frequencies. The calibration in this case can be accomplished through the value of the spectral radius at a given sampling frequency, say ${}^{ED2}\rho(\pi)$ in (2.42).

The spectral response for small sampling frequencies Ω is characterized by the asymptotic limits

$$\xi_d(\Omega) = \frac{\alpha^2}{2}\Omega^3 + \mathcal{O}(\Omega^4)\,, \tag{2.44}$$

$$e_\Omega(\Omega) = \tfrac{1}{2}\left(\alpha - \frac{1}{6}\right)\Omega^2 + \mathcal{O}(\Omega^3)\,, \tag{2.45}$$

as $\Omega \to 0$, after some algebraic manipulations involving (2.41). The third-order accuracy of the combination $\alpha = 1/6$ becomes apparent from these two last expressions. This property, however, does not extend to the extensions to nonlinear elastodynamics presented in the next section. Furthermore, we observe that the numerical dissipation introduced in the

system, measured in terms of the damping ratio ξ_d is of the order Ω^3 for small values of Ω (note that the dissipation function $\mathcal{D}$ in (2.22) is of order Δt^3).

Figure 2.3 depicts the results of this spectral analysis of the ED-2 scheme. As in Figure 2.2 for the ED-1 scheme, the distributions of the damping ratio $\xi_d(\Omega)$, relative frequency error $e_\Omega(\Omega)$ and spectral radius $\rho(\Omega)$ are shown continuously in the algorithmic parameter α (the 3D plots in the left column) and for fixed values of α (the 2D plots in the right column, sections of the previous 3D plots for fixed α). As expected and shown above, we observe the absence of numerical dissipation ($\xi_d(\Omega) \equiv 0$ or, equivalently, $\rho(\Omega) = 1$) for the conservative case $\alpha = 0$. Increasing the algorithmic parameter α increases the numerical dissipation, characterized by increasing values of $\xi_d(\Omega)$ for a given sampling sampling frequency Ω. Similarly, we observe that for large sampling frequencies the relative frequency error is negative ($e_\Omega \leq 0$), indicating that the computed frequencies are diminished compared with the exact value Ω for this range of frequencies (i.e., the computed periods are elongated, as defined above). For small frequencies Ω, the relative frequency error is positive for large values of the algorithmic parameter α. The second-order accuracy of the method for any value of α (third-order for $\alpha = 1/6$) is also apparent by the zero slope of the curves in the right column, reflecting the limit values obtained analytically in (2.44) and (2.45) for small Ω.

3. Extensions to Nonlinear Elastodynamics

We address in this section the extension of the developments presented in the previous section to the general system of nonlinear finite elastodynamics. The challenges in this task can be stated as:

- **i.** To maintain the energy dissipative character of the schemes for any elastic potential, including the control on the numerical dissipation (through the appropriate algorithmic parameters) and their second-order accuracy in time.
- **ii.** To preserve exactly the conservation laws of the momentum maps and corresponding relative equilibria of the underlying continuum system, thus preserving fundamental qualitative features of the phase dynamics.
- **iii.** To avoid costly multi-stage implementations, as indicated above.

The time-stepping algorithms developed in the previous section where focused in the construction of linear schemes given the linearity of the underlying problem, resulting in the two-stage formulae of the second-order ED-2 scheme. Therefore, a direct application of the previous algorithms to the nonlinear problem does not address the three aforementioned challenges, including especially the conservation of angular momentum. Nevertheless, we show in this section that these objectives can be accomplished following similar arguments in the construction of the numerical schemes. In this way, after defining briefly the problem

under consideration in Section 3.1, we formulate in Section 3.2 a new second-order energy-dissipative/momentum-conserving time-stepping algorithm for nonlinear elastodynamics.

3.1. Problem definition

We are interested in the integration in time of the deformation $\boldsymbol{\varphi} : \mathcal{B} \times [0,T] \to \mathbb{R}^{n_{\text{dim}}}$ and material velocity $\boldsymbol{v} : \mathcal{B} \times [0,T] \to \mathbb{R}^{n_{\text{dim}}}$ ($n_{\text{dim}} = 1, 2$ or 3) of a solid $\mathcal{B} \subset \mathbb{R}^{n_{\text{dim}}}$ with material particles denoted by $\boldsymbol{X} \in \mathcal{B}$ and a time interval $[0,T]$. The weak form of the governing equations (balance of linear momentum) reads

$$\left.\begin{aligned} \dot{\boldsymbol{\varphi}} &= \boldsymbol{v} \,, \\ \int_{\mathcal{B}} \rho_o \dot{\boldsymbol{v}} \cdot \delta\boldsymbol{\varphi} \, d\mathcal{B} + \int_{\mathcal{B}} \boldsymbol{S} : \boldsymbol{F}^T \, \text{GRAD}(\delta\boldsymbol{\varphi}) \, d\mathcal{B} &= \int_{\mathcal{B}} \rho_o \boldsymbol{B} \cdot \delta\boldsymbol{\varphi} \, d\mathcal{B} + \int_{\partial_T \mathcal{B}} \bar{\boldsymbol{T}} \cdot \delta\boldsymbol{\varphi} \, d\Gamma \,, \end{aligned}\right\} \tag{3.1}$$

for all admissible variations $\delta\boldsymbol{\varphi}$ satisfying homogeneous essential boundary conditions $\delta\boldsymbol{\varphi} = 0$ on $\partial_u \mathcal{B}$ (the part of the boundary with imposed deformations), as usual. We have denoted in (3.1) the reference density of the solid by $\rho_o > 0$, the deformation gradient by $\boldsymbol{F} := \text{GRAD}\, \boldsymbol{\varphi}$ (with material gradient $\text{GRAD}[\cdot]$), the second Piola-Kirchhoff stress tensor by $\boldsymbol{S}$, the external body force $\boldsymbol{B}$, and imposed tractions $\bar{\boldsymbol{T}}$ on $\partial_T \mathcal{B}$ has been employed in (3.1). The hyperelastic relation

$$\boldsymbol{S} = 2 \frac{\partial W}{\partial \boldsymbol{C}} \,. \tag{3.2}$$

in terms of a general stored energy function $W = \hat{W}(\boldsymbol{C})$, with $\boldsymbol{C} := \boldsymbol{F}^T \boldsymbol{F}$ (by frame indifference).

As described in Part I of this work, the system of equations (3.1) defines an infinite dimensional Hamiltonian system, exhibiting the following conservation laws:

i. *Conservation of energy.* For the Neumann problem with no applied forces (i.e., $\boldsymbol{B} = \bar{\boldsymbol{T}} = 0$ and $\partial_u \mathcal{B} = \emptyset$), the total energy is conserved, that is,

$$H(\boldsymbol{\varphi}, \boldsymbol{p}(\boldsymbol{v})) = \int_{\mathcal{B}} \tfrac{1}{2} \, \rho_o \, \|\boldsymbol{v}\|^2 \, d\mathcal{B} + \int_{\mathcal{B}} W(\boldsymbol{C}(\boldsymbol{\varphi})) \, d\mathcal{B} = \textit{ constant} \,, \tag{3.3}$$

for the Hamiltonian $H(\cdot)$ in terms of the linear momentum density $\boldsymbol{p} := \rho_o \boldsymbol{v}$.

ii. *Conservation of linear momentum.* The invariance of the Hamiltonian (3.3) under rigid translations leads to the conservation law

$$\boldsymbol{l} := \int_{\mathcal{B}} \rho_o \, \boldsymbol{v} \, d\mathcal{B} = \textit{ constant} \,, \tag{3.4}$$

when the boundary conditions and loading exhbit this invariance (e.g., $\boldsymbol{B} = \bar{\boldsymbol{T}} = 0$ and $\partial_u \mathcal{B} = \emptyset$).

iii. *Conservation of angular momentum.* The invariance of the Hamiltonian (3.3) under rigid rotations leads to the conservation law

$$\boldsymbol{J} := \int_{\mathcal{B}} \rho_o \, \boldsymbol{\varphi} \times \boldsymbol{v} \, d\mathcal{B} = \; constant \, , \tag{3.5}$$

when the boundary conditions and loading share this invariance (e.g., $\boldsymbol{B} = \bar{\boldsymbol{T}} = 0$ and $\partial_u \mathcal{B} = \emptyset$). In (3.5) we have made use of the cross product $\times$ of two vectors in $\mathbb{R}^3$, or its corresponding embedding in lower dimensions.

As considered in detail in Part I, these symmetries lead also to the existence of relative equilibria (see e.g. MARSDEN [1992]), that is, solutions of the general systems of equations (3.1) consisting of a rigid-body motion (rigid rotation and translation) superposed to a fixed equilibrium deformation. We refer to Part I of this work and references therein for details.

We consider a general isoparametric finite element approximation of the continuum equations (3.1) through the interpolations

$$\boldsymbol{\varphi} = \boldsymbol{X} + \sum_{A=1}^{n_{node}} N_A(\boldsymbol{X}) \; \boldsymbol{d}^A(t) \quad \text{and} \quad \boldsymbol{v} = \sum_{A=1}^{n_{node}} N_A(\boldsymbol{X}) \; \boldsymbol{v}^A(t) \, , \tag{3.6}$$

in terms of the shape function $N_A(\cdot)$ for n_{node} nodes, nodal displacements $\boldsymbol{d} = \left\{ \boldsymbol{d}^{1^T} \; \boldsymbol{d}^{2^T} \ldots \right\}^T \in \mathbb{R}^{n_{dof}}$, and nodal velocities $\boldsymbol{v} = \left\{ \boldsymbol{v}^{1^T} \; \boldsymbol{v}^{2^T} \ldots \right\}^T \in \mathbb{R}^{n_{dof}}$. Standard procedures lead to the nonlinear system of spatially discrete equations

$$\left.\begin{aligned} \dot{\boldsymbol{d}} &= \boldsymbol{v} \\ \boldsymbol{M} \dot{\boldsymbol{v}} &= -\int_{\mathcal{B}} \boldsymbol{B}^T \boldsymbol{S} \; d\mathcal{B} + \boldsymbol{f}_{ext}(t) \end{aligned}\right\} \tag{3.7}$$

in terms of the (consistent) mass matrix

$$\boldsymbol{M} = [M_{AB} \; \mathbf{1}] \quad \text{for} \quad M_{AB} = \int_{\mathcal{B}} \rho_o \; N_A \; N_B \; d\mathcal{B} \in \mathbb{R}^{n_{\text{dim}} \times n_{\text{dim}}} \, , \tag{3.8}$$

(for $A, B = 1, n_{node}$) and the linearized strain operator ($\boldsymbol{B}\delta\boldsymbol{d} = \text{sym}[\boldsymbol{F}^T \, \text{GRAD} \, \delta\boldsymbol{\varphi}]$ for a deformation variation $\delta\boldsymbol{\varphi}$ and corresponding nodal variations $\delta\boldsymbol{d}$), and external forces $\boldsymbol{f}_{ext}$ (including possibly imposed boundary displacements). This system of ODE's is supplemented by the initial conditions (2.3) as in the linear case. The same conservation laws (3.3)-(3.5) are inherited by the spatially discrete system (3.7).

3.2. Energy dissipative, momentum conserving schemes

Following the developments in Section 2 for the linear case, we consider the following temporal discretization of the nonlinear system of equations (3.7)

$$\left.\begin{aligned} \frac{\boldsymbol{d}^A_{n+1} - \boldsymbol{d}^A_n}{\Delta t} &= \boldsymbol{v}^A_{n+\frac{1}{2}} + \boldsymbol{g}^A_{diss} \,, \quad (A = 1, n_{node}) \,, \\ \boldsymbol{M} \frac{\boldsymbol{v}_{n+1} - \boldsymbol{v}_n}{\Delta t} &= - \int_{\mathcal{B}} \boldsymbol{B}^T_{n+\frac{1}{2}} \boldsymbol{S} \, dV + \tilde{\boldsymbol{f}}_{ext} \,, \end{aligned}\right\} \tag{3.9}$$

for a typical time increment $[t_n, t_{n+1}]$, and mid-point evaluations of the velocities $\boldsymbol{v}_{n+1/2} = (\boldsymbol{v}_{n+1} + \boldsymbol{v}_n)/2$, and the linearized strain operator $\boldsymbol{B}_{n+1/2}$ (at $\boldsymbol{\varphi}_{n+1/2} = (\boldsymbol{\varphi}_{n+1} + \boldsymbol{\varphi}_n)/2$). As in the linear case (2.8), the external force vector is approximated through a general expression $\tilde{\boldsymbol{f}}_{ext}$ (e.g. the second-order expression $\tilde{\boldsymbol{f}}_{ext} = \boldsymbol{f}_{ext}(t_{n+\frac{1}{2}})$). The stresses $\boldsymbol{S}$ in $(3.9)_2$ are given by

$$\boldsymbol{S} = \boldsymbol{S}_{cons} + 2 \frac{\mathcal{D}_W}{\|\boldsymbol{C}_{n+1} - \boldsymbol{C}_n\|} \boldsymbol{N} \,, \quad \text{for} \quad \boldsymbol{N} := \frac{\boldsymbol{C}_{n+1} - \boldsymbol{C}_n}{\|\boldsymbol{C}_{n+1} - \boldsymbol{C}_n\|} \,, \tag{3.10}$$

with the Euclidean norm of a rank-two tensor $\|\boldsymbol{C}\|^2 := C_{ij} C_{ij}$. Here, $\boldsymbol{S}_{cons}$ denotes a conserving approximation of the stress formula (3.2), that is, satisfying the relation

$$\boldsymbol{S}_{cons} : \tfrac{1}{2} (\boldsymbol{C}_{n+1} - \boldsymbol{C}_n) = W(\boldsymbol{C}_{n+1}) - W(\boldsymbol{C}_n) \,. \tag{3.11}$$

The simulations presented in Section 4 consider the expression

$$\boldsymbol{S}_{cons} = 2 \frac{W(\boldsymbol{C}_{n+1}) - W(\boldsymbol{C}_n)}{\|\boldsymbol{C}_{n+1} - \boldsymbol{C}_n\|} \boldsymbol{N} + 2 \left[\boldsymbol{I} - \boldsymbol{N} \otimes \boldsymbol{N} \right] \partial_{\boldsymbol{C}} W \left(\frac{\boldsymbol{C}_{n+1} + \boldsymbol{C}_n}{2} \right) \,, \tag{3.12}$$

with the well-defined limit

$$\boldsymbol{S}_{cons} = 2 \, \partial_{\boldsymbol{C}} W \left(\frac{\boldsymbol{C}_{n+1} + \boldsymbol{C}_n}{2} \right) \qquad \text{for} \quad \boldsymbol{C}_n = \boldsymbol{C}_{n+1} \,, \tag{3.13}$$

first proposed in SIMO & GONZALEZ [1994]. As noted in Remark 5.1.2 of Part I of this work, the discrete stress formula (3.10) can be written in more general form as

$$\boldsymbol{S} = \hat{\boldsymbol{S}} + \left[2 \frac{W(\boldsymbol{C}_{n+1}) - W(\boldsymbol{C}_n) + \mathcal{D}_W}{\|\boldsymbol{C}_{n+1} - \boldsymbol{C}_n\|} - \hat{\boldsymbol{S}} : \boldsymbol{N} \right] \boldsymbol{N} \,, \tag{3.14}$$

for a general second-order approximation $\hat{\boldsymbol{S}}$ of (3.13), while maintaining the dissipation/conservation properties described in this section.

The dissipative contributions $\boldsymbol{g}_{diss}$ to the velocity equation $(3.9)_1$ are defined nodally by $\boldsymbol{g}^B_{diss} \in \mathbb{R}^{n_{\text{dim}}}$ through the solution of the system of equations

$$\sum_{B=1}^{n_{node}} \boldsymbol{M}_{AB}\, \boldsymbol{g}^B_{diss} = \int_{\mathcal{B}} N_A\, \frac{\mathcal{D}_v}{\|\boldsymbol{v}_{n+1}\| - \|\boldsymbol{v}_n\|}\, \frac{\boldsymbol{v}_{n+1} + \boldsymbol{v}_n}{\|\boldsymbol{v}_{n+1}\| + \|\boldsymbol{v}_n\|}\, d\mathcal{B}\,, \tag{3.15}$$

for a dissipation function $\mathcal{D}_v$. We note the equality

$$\sum_{A,B=1}^{n_{node}} (\boldsymbol{v}^A_{n+1} - \boldsymbol{v}^A_n) \cdot \boldsymbol{M}_{AB}\, \boldsymbol{g}^B_{diss} = \int_{\mathcal{B}} \mathcal{D}_v\, d\mathcal{B}\,. \tag{3.16}$$

similar to $(2.10)_2$ for the linear case. In this way, multiplying equation $(3.9)_1$ by $\boldsymbol{M}(\boldsymbol{v}_{n+1} - \boldsymbol{v}_n)$ and $(3.9)_2$ by $(\boldsymbol{d}_{n+1} - \boldsymbol{d}_n)$, we arrive at the discrete energy evolution equation

$$H^h_{n+1} - H^h_n = \tilde{\boldsymbol{f}}_{ext} \cdot (\boldsymbol{d}_{n+1} - \boldsymbol{d}_n) - \int_{\mathcal{B}} [\mathcal{D}_v + \mathcal{D}_W]\; d\mathcal{B}\,, \tag{3.17}$$

after some algebraic manipulations. Here H^h_n and H^h_{n+1} correspond to the exact Hamiltonian function (3.3) evaluated with the finite element solution at times t_n and t_{n+1}, respectively. The dissipative character of the resulting numerical scheme for the force-free case $\tilde{\boldsymbol{f}}_{ext} = 0$ is then concluded if we have $\mathcal{D}_v + \mathcal{D}_W \geq 0$. We note that the two dissipation functions $\mathcal{D}_W$ and $\mathcal{D}_v$ are to be defined only locally at the quadrature points since they appear under an integral sign. This important observation is employed below to arrive to efficient second-order schemes.

In addition, the specific form of the dissipative terms in $(3.9)_1$ and (3.15) leads to approximations conserving the momenta. Indeed, denoting by $\boldsymbol{l}^h_{n+1}$ and $\boldsymbol{l}^h_n$ the linear momentum of the finite element solution at t_n and t_{n+1} respectively (i.e., formula (3.4) with the finite element fields) and using $(3.9)_2$, we arrive at the relation

$$\begin{aligned}
(\boldsymbol{l}^h_{n+1} - \boldsymbol{l}^h_n) \cdot \boldsymbol{a} &= \int_{\mathcal{B}} \boldsymbol{a} \cdot \rho_o(\boldsymbol{v}_{n+1} - \boldsymbol{v}_n)\; d\mathcal{B} \\
&= -\int_{\mathcal{B}} \boldsymbol{S} : \boldsymbol{F}^T_{n+\frac{1}{2}} \underbrace{\text{GRAD}\,[\boldsymbol{a}]}_{0}\; d\mathcal{B} + \Delta t \left(\sum_{A=1}^{n_{node}} \tilde{\boldsymbol{f}}^A_{ext} \right) \cdot \boldsymbol{a} \\
&= \Delta t \left(\sum_{A=1}^{n_{node}} \tilde{\boldsymbol{f}}^A_{ext} \right) \cdot \boldsymbol{a} \qquad \forall \boldsymbol{a} \in \mathbb{R}^{n_{\text{dim}}}\,,
\end{aligned} \tag{3.18}$$

thus leading to the conservation of the linear momentum when $\tilde{\boldsymbol{f}}_{ext} = 0$ (note that this implies no imposed boundary displacements as well). Similarly, denoting by $\boldsymbol{J}^h_{n+1}$ and $\boldsymbol{J}^h_n$ the linear momentum of the finite element solution at t_n and t_{n+1} respectively (i.e.,

formula (3.5) with the finite element fields) and using (3.9), we arrive after some algebraic manipulations at the relation

$$\begin{aligned}(\boldsymbol{J}^h_{n+1} - \boldsymbol{J}^h_n)\cdot\boldsymbol{a} &= \int_{\mathcal{B}} \boldsymbol{a}\cdot\rho_o(\boldsymbol{\varphi}_{n+1}\times\boldsymbol{v}_{n+1} - \boldsymbol{\varphi}_n\times\boldsymbol{v}_n)\,d\mathcal{B}\\ &= -\int_{\mathcal{B}} \underbrace{\boldsymbol{F}_{n+\frac{1}{2}}\boldsymbol{S}\boldsymbol{F}^T_{n+\frac{1}{2}}}_{symmetric} : \underbrace{\hat{\boldsymbol{a}}}_{skew}\; d\mathcal{B} + \Delta t\;\tilde{\boldsymbol{m}}_{ext}\cdot\boldsymbol{a}\\ &= \Delta t\;\tilde{\boldsymbol{m}}_{ext}\cdot\boldsymbol{a} \qquad \forall\boldsymbol{a}\in\mathbb{R}^{n_{\text{dim}}}\,,\end{aligned} \tag{3.19}$$

where $\hat{\boldsymbol{a}}$ denotes the skew-symmetric tensor with axial vector $\boldsymbol{a}$, and $\tilde{\boldsymbol{m}}_{ext}$ is the moment of the external loading, given by

$$\tilde{\boldsymbol{m}}_{ext} := \int_{\mathcal{B}} \boldsymbol{\varphi}_{n+\frac{1}{2}}\times\rho_o\,\tilde{\boldsymbol{B}}\,d\mathcal{B} + \int_{\partial\mathcal{B}} \boldsymbol{\varphi}_{n+\frac{1}{2}}\times\tilde{\boldsymbol{T}}\,d\Gamma\,, \tag{3.20}$$

where $\tilde{\boldsymbol{B}}$ and $\tilde{\boldsymbol{T}}$ denotes the temporal discretization assumed for the external loads, the later consisting of all the surface loads on the boundary $\partial\mathcal{B}$, including the reactions at the boundary $\partial_u\mathcal{B}$ with imposed displacements at the mid-configuration $\boldsymbol{\varphi}_{n+1/2}$. Therefore, the conservation of the angular momentum for $\tilde{\boldsymbol{m}}_{ext} = 0$ (including no imposed boundary displacements as well) is concluded.

The above developments follow the same arguments as the ones presented in Part I of this work (hence the conciseness in the presentation) for the analysis of similar time-stepping schemes but in combination with a lumped form of the mass matrix $\boldsymbol{M}$ and dissipation function in the velocities. In the same way, we can prove that the relative equilibria of the discrete system (3.7) (now involving a consistent form of the centrifugal body forces in the equilibrium configurations) are also conserved by the time-stepping scheme. We refer the reader to this reference for a proof and further details. We summarize these properties in the following proposition.

Proposition 3.1 *The numerical scheme (3.9), with (3.10) and (3.15), possesses the following conservation/dissipation properties for the Neumann problem of nonlinear elastodynamics (i.e. $\tilde{\boldsymbol{f}}_{ext} = 0$ with $\partial_u\mathcal{B} = \emptyset$):*

1. *The discrete $\boldsymbol{l}^h$ linear and angular momenta $\boldsymbol{J}^h$ are conserved. That is, we have*

$$\boldsymbol{l}^h_{n+1} = \boldsymbol{l}^h_n \qquad \textit{and} \qquad \boldsymbol{J}^h_{n+1} = \boldsymbol{J}^h_n \tag{3.21}$$

   unconditionally in the time step Δt.

2. *The total energy evolves as*

$$H^h_{n+1} - H^h_n = -\int_{\mathcal{B}} [\mathcal{D}_v + \mathcal{D}_W]\;d\mathcal{B}\,. \tag{3.22}$$

Hence the scheme is dissipative unconditionally in Δt and the elastic potential $W(\cdot)$ if $\mathcal{D} := \mathcal{D}_v + \mathcal{D}_W \geq 0$.

3. *The discrete dynamical system preserves the relative equilibria.*

The numerical scheme is then totally determined once the dissipation functions $\mathcal{D}_W$ and $\mathcal{D}_v$ are defined at the quadrature points. In this context, a first-order energy-dissipative momentum-conserving scheme was presented in Part I of this work, with the dissipation functions

$$\left.\begin{aligned} \mathcal{D}_W &= \chi_1 \, \tfrac{1}{2} \, (\boldsymbol{C}_{n+1} - \boldsymbol{C}_n) : \tfrac{1}{4}\widehat{\mathbb{C}}_n \, (\boldsymbol{C}_{n+1} - \boldsymbol{C}_n) \geq 0 \\ \mathcal{D}_v &= \chi_2 \, \tfrac{1}{2} \, \rho_o \, (\|\boldsymbol{v}_{n+1}\| - \|\boldsymbol{v}_n\|)^2 \geq 0 \end{aligned}\right\} \tag{3.23}$$

for two algorithmic parameters $\chi_1 \geq 0$ and $\chi_2 \geq 0$, and a positive (semi-)definite tensor $\widehat{\mathbb{C}}_n$, e.g. $\widehat{\mathbb{C}}_n = 4\partial^2_{CC} W|_n$ (or its convexification; see e.g. DACOROGNA [1989], page 35), leading a first-order scheme, referred to as EDMC-1. More precisely, we presented in this reference a variant involving a lumped mass matrix with an equivalent nodally-based definition of the dissipation function $\mathcal{D}_v$ that leads to a very efficient numerical implementation of the final discrete equations, involving the solution of a system of n_{dof} equations with independent nodal updates for the nodal velocities corresponding to equation $(3.9)_1$. The expressions (3.23) are analogous to (2.18). In this way, the resulting scheme can be considered the extension to the nonlinear case of the energy-dissipative ED-1 scheme described in Section 2.1.1 for linear elastodynamics. We develop in the next section a second-order energy-dissipative momentum-conserving scheme, denoted by EDMC-2, extending the energy dissipative ED-2 schemes formulated in Section 2.1.2 for the linear problem.

3.2.1. A second-order energy decaying scheme (EDMC-2)

As noted in the beginning of this section, one of the challenges in the formulation of efficient time-stepping algorithms is to avoid multi-stage formulas like the ED-2 scheme developed in Section 2.1.2 for linear elastodynamics, thus avoiding the doubling of the number of unknowns (i.e., nodal displacements and velocities) for each additional stage. The key observation is again that the dissipation functions $\mathcal{D}_v$ and $\mathcal{D}_W$ (see e.g. (3.22)) need to be defined locally at the quadrature points of the finite element implementation only. Therefore, and motivated by the developments of Section 2.1.2 for the linear case, we introduce the definitions

$$\mathcal{D}_W = \tfrac{1}{2} \, (\tilde{\boldsymbol{C}}_n - \boldsymbol{C}_n) : \tfrac{1}{4}\widehat{\mathbb{C}}_n \, (\boldsymbol{C}_{n+1} - \boldsymbol{C}_n) \, , \tag{3.24}$$

for an intermediate "strain measure" $\tilde{\boldsymbol{C}}_n$, second-order approximation in time of $\boldsymbol{C}_n$, and, introducing the notation $v_n := \|\boldsymbol{v}_n\|$ and $v_{n+1} := \|\boldsymbol{v}_{n+1}\|$,

$$\mathcal{D}_v = \tfrac{1}{2} \, (\tilde{v}_n - v_n) \, \rho_o \, (v_{n+1} - v_n) \, , \tag{3.25}$$

for an intermediate scalar value $\tilde{v}_n$, second-order approximation in time of $v_n := \|\boldsymbol{v}_n\|$. That is, we require

$$\tilde{\boldsymbol{C}}_n = \boldsymbol{C}_n + \mathcal{O}(\Delta t^2) \quad \text{and} \quad \tilde{v}_n = v_n + \mathcal{O}(\Delta t^2) \,. \tag{3.26}$$

We note that the use of the intermediate values $\tilde{\boldsymbol{C}}_n$ and $\tilde{v}_n$ does not require the introduction of new nodal displacements and velocities (say $\tilde{\boldsymbol{d}}_n$ and $\tilde{\boldsymbol{v}}_n$) as in the linear case. These quantities are to be understood as numerical terms that through the definitions introduced next lead to a dissipative numerical approximation being second-order in time.

Similarly, the only property required to the fourth-order tensor $\widehat{\mathbb{C}}_n$ introduced in (3.24) is its positive definiteness. The consideration of a constant $\widehat{\mathbb{C}}_n$ in the time step simplifies considerably the final numerical implementation, especially the consistent linearization of the resulting equations. In this way, we consider $\widehat{\mathbb{C}}_n = 4\partial^2_{\boldsymbol{C}\boldsymbol{C}} W|_n$, (or its convexification) or simply $\widehat{\mathbb{C}}_n = \kappa_n \mathbb{I}$ for a scalar parameter $\kappa_n > 0$ and the fourth-order identity matrix $\mathbb{I}$. A value of $\kappa_n = 2\mu$ (the initial shear modulus) has been assumed in the simulations presented in Section 4 involving a compressible Neo-Hookean finite elastic model. We note the residual character of the definitions (3.24) and (3.25) (through the proper definition of the intermediate values $\tilde{\boldsymbol{C}}_n$ and $\tilde{v}_n$, as developed below), and conclude the consistency of these different alternatives in the definition of $\widehat{\mathbb{C}}_n$.

A simple definition of the intermediate tensor $\tilde{\boldsymbol{C}}_n$ is given in the form

$$\tilde{\boldsymbol{C}}_n = \boldsymbol{C}_n + \tilde{\beta}_n \, (\boldsymbol{C}_{n+1} - \boldsymbol{C}_n) \,, \tag{3.27}$$

for an unknown scalar parameter $\tilde{\beta}_n$. We note that both $\boldsymbol{C}_n$ and $\boldsymbol{C}_{n+1}$ are known in a typical iterative procedure (e.g. Newton-Raphson) when solving the nonlinear system of equations (3.9). The requirement $(3.26)_1$ for a second-order scheme translates then to

$$\tilde{\beta}_n = \mathcal{O}(\Delta t) \,, \tag{3.28}$$

since $\boldsymbol{C}_{n+1} - \boldsymbol{C}_n = \mathcal{O}(\Delta t)$. The numerical scheme reduces then to the definition of the two scalars $\tilde{\beta}_n$ and $\tilde{v}_n$ at each quadrature point.

Motivated by the developments in Section 2.1.2 for the linear case, equations (2.21) in particular, we introduce the definitions

$$\left.\begin{aligned} \tilde{\beta}_n &= \alpha \, \frac{\Delta t}{h} \, (v_{n+1} - \tilde{v}_n) \,, \\ \tilde{v}_n &= v_n - \alpha \, \frac{\Delta t}{h} \, c^2 \, \|\boldsymbol{C}_{n+1} - \boldsymbol{C}_n\|^2 (1 - \tilde{\beta}_n) \,, \end{aligned}\right\} \tag{3.29}$$

for an algorithmic parameter α, a length scale h (e.g. $h = \sqrt[n_{\text{dim}}]{\text{quadrature point volume}} = \sqrt[n_{\text{dim}}]{j}$, for j = determinant of isoparametric mapping $\times$ quadrature weight) and

$$c^2 := \frac{\hat{\kappa}}{\rho_o} \,, \quad \text{where} \quad \hat{\kappa} := \frac{(\boldsymbol{C}_{n+1} - \boldsymbol{C}_n) : \frac{1}{4}\widehat{\mathbb{C}} \, (\boldsymbol{C}_{n+1} - \boldsymbol{C}_n)}{\|\boldsymbol{C}_{n+1} - \boldsymbol{C}_n\|^2} \,. \tag{3.30}$$

The dimensional consistency of the final equations (3.29) can be verified. We also observe that the required order conditions (3.26) and (3.28) are satisfied. In fact, we even have

$$\tilde{\beta} = \mathcal{O}(\lambda_{CFL}\ \Delta t) \quad \text{and} \quad \tilde{v}_n = v_n + \mathcal{O}(\lambda_{CFL}\ \Delta t^2) \qquad \text{for} \quad \lambda_{CFL} = c\frac{\Delta t}{h}\ , \tag{3.31}$$

that is, a "Courant parameter" in terms of the speed value c defined in (3.30). The expressions (3.30) are simple linear equations in the two unknown scalars $\tilde{\beta}_n$ and $\tilde{v}_n$, with the closed-form solution

$$\tilde{\beta}_n = \frac{1}{\tilde{\Delta}}\ \alpha\frac{\Delta t}{h}\ \left[v_{n+1} - v_n + \alpha\ \frac{\Delta t}{h}\ c^2\ \|\boldsymbol{C}_{n+1} - \boldsymbol{C}_n\|^2\right]\ , \tag{3.32}$$

and

$$\tilde{v}_n = \frac{1}{\tilde{\Delta}}\ \left[v_n - \alpha\ \left(1 - \alpha\ \frac{\Delta t}{h}\ v_{n+1}\right)\frac{\Delta t}{h}\ c^2\ \|\boldsymbol{C}_{n+1} - \boldsymbol{C}_n\|^2\right]\ , \tag{3.33}$$

for

$$\tilde{\Delta} = 1 + \alpha^2\ \lambda_{CFL}^2\ \|\boldsymbol{C}_{n+1} - \boldsymbol{C}_n\|^2$$

with $\tilde{\beta}_n = 0$ and $\tilde{v}_n = v_n$ for $\|\boldsymbol{C}_{n+1} - \boldsymbol{C}_n\| = 0$ and $\|\boldsymbol{v}_{n+1}\| = \|\boldsymbol{v}_n\|$.

The motivation behind the definitions (3.30) is the non-negative character of the combination $\mathcal{D}_W + \mathcal{D}_v$ appearing in the final expression (3.22) of the total dissipation, as in the linear case considered in Section 2.1.2 for the ED-2 scheme. This property is achieved through the cross-type definitions of $\tilde{\beta}_n$ and $\tilde{v}_n$ appearing in expressions (3.30). In fact, we have

$$\begin{aligned}
\mathcal{D}_v + \mathcal{D}_W &= \tfrac{1}{2}\ (\tilde{v}_n - v_n)\ \rho_o\ (v_{n+1} - v_n) + \tfrac{1}{2}\ (\tilde{\boldsymbol{C}}_n - \boldsymbol{C}_n) : \tfrac{1}{4}\widehat{\mathbb{C}}_n\ (\boldsymbol{C}_{n+1} - \boldsymbol{C}_n) \\
&= \tfrac{1}{2}\ \rho_o\ (\tilde{v}_n - v_n)^2 + \tfrac{1}{2}\ (\tilde{\boldsymbol{C}}_n - \boldsymbol{C}_n) : \tfrac{1}{4}\widehat{\mathbb{C}}_n\ (\tilde{\boldsymbol{C}}_n - \boldsymbol{C}_n) \\
&\quad - \tfrac{1}{2}\ (\tilde{v}_n - v_n)\ \rho_o\ (\tilde{v}_n - v_{n+1}) - \tfrac{1}{2}\ (\tilde{\boldsymbol{C}}_n - \boldsymbol{C}_n) : \tfrac{1}{4}\widehat{\mathbb{C}}_n\ (\tilde{\boldsymbol{C}}_n - \boldsymbol{C}_{n+1}) \\
&= \tfrac{1}{2}\ \rho_o\ (\tilde{v}_n - v_n)^2 + \tfrac{1}{2}\ (\tilde{\boldsymbol{C}}_n - \boldsymbol{C}_n) : \tfrac{1}{4}\widehat{\mathbb{C}}_n\ (\tilde{\boldsymbol{C}}_n - \boldsymbol{C}_n) \\
&\quad - \tfrac{1}{2}\ (\tilde{v}_n - v_n)\ \rho_o\ (\tilde{v}_n - v_{n+1}) - \tfrac{1}{2}\ \underbrace{(\tilde{\boldsymbol{C}}_n - \boldsymbol{C}_n)}_{=\,\tilde{\beta}_n(\boldsymbol{C}_{n+1}-\boldsymbol{C}_n)} : \tfrac{1}{4}\widehat{\mathbb{C}}_n\ \underbrace{(\tilde{\boldsymbol{C}}_n - \boldsymbol{C}_{n+1})}_{=\,-(1-\tilde{\beta}_n)(\boldsymbol{C}_{n+1}-\boldsymbol{C}_n)} \\
&= \tfrac{1}{2}\ \rho_o\ (\tilde{v}_n - v_n)^2 + \tfrac{1}{2}\ (\tilde{\boldsymbol{C}}_n - \boldsymbol{C}_n) : \tfrac{1}{4}\widehat{\mathbb{C}}_n\ (\tilde{\boldsymbol{C}}_n - \boldsymbol{C}_n) \\
&\quad - \tfrac{1}{2}\ (\tilde{v}_n - v_n)\ \rho_o\ (\tilde{v}_n - v_{n+1}) - \tfrac{1}{2}\ \underbrace{\tilde{\beta}_n}_{=\,\alpha\frac{\Delta t}{h}(v_{n+1}-\tilde{v}_n)\ \text{by}\ (3.29)_1}\ (1 - \tilde{\beta}_n)\ c^2\rho_o\ \|\boldsymbol{C}_{n+1} - \boldsymbol{C}_n\|^2 \\
&= \tfrac{1}{2}\ \rho_o\ (\tilde{v}_n - v_n)^2 + \tfrac{1}{2}\ (\tilde{\boldsymbol{C}}_n - \boldsymbol{C}_n) : \tfrac{1}{4}\widehat{\mathbb{C}}_n\ (\tilde{\boldsymbol{C}}_n - \boldsymbol{C}_n)
\end{aligned}$$

$$- \tfrac{1}{2} \Big[\underbrace{(\tilde{v}_n - v_n) + \alpha\,(1-\tilde{\beta}_n)\,c^2\,\frac{\Delta t}{h}\,\|\tilde{\boldsymbol{C}}_{n+1} - \boldsymbol{C}_n\|^2}_{=0 \text{ by } (3.29)_2} \Big] \rho_o\,(\tilde{v}_n - v_{n+1})$$

$$= \tfrac{1}{2}\,\rho_o\,(\tilde{v}_n - v_n)^2 + \tfrac{1}{2}\,(\tilde{\boldsymbol{C}}_n - \boldsymbol{C}_n) : \tfrac{1}{4}\widehat{\mathbb{C}}_n\,(\tilde{\boldsymbol{C}}_n - \boldsymbol{C}_n) \geq 0\,, \tag{3.34}$$

since $\rho_o > 0$ and $\widehat{\mathbb{C}}_n$ is positive semi-definite. Furthermore, the relation (3.34) holds unconditionally in Δt and, perhaps more importantly, unconditionally on the elastic potential $W(\cdot)$.

We emphasize once more that the final numerical scheme reduces to the evaluation of proper dissipation functions at the quadrature points. This is simply accomplished through the (linear) evaluation (3.32)-(3.33) of two scalar parameters. The implementation involves then the solution of a $2 \cdot n_{dof}$ algebraic system of equations in $\boldsymbol{d}_{n+1}$ and $\boldsymbol{v}_{n+1}$ only, and not $4 \cdot n_{dof}$ equations as it would be the case in a two-stage scheme. Appendix I describes the details of the final numerical implementation of the proposed scheme. The dissipation/conservation properties summarized in Proposition 3.1, as well as the second-order accuracy in time of the resulting scheme, is confirmed in the numerical simulations presented in the following section.

Remark 3.1. We note that the need to introduce the length scale parameter h in (3.29) is a consequence of the definition of the dissipation functions at the level of the quadrature points, with temporal relations involving strains and velocities (thus the need of the length parameter for dimensional consistency). This situation does not apply to other nonlinear Hamiltonian systems, where the developments presented above for the system of nonlinear elastodynamics generalize. For example, for the simpler model problem of a nonlinear spring with elastic potential $V(l)$ (l = spring length), fixed at one end and with a point mass m at the other end free of other external forces, as considered in Part I of this work, the EDMC-2 scheme reads

$$\left.\begin{aligned} \frac{1}{\Delta t}\,(q_{n+1} - q_n) &= v_{n+\frac{1}{2}} + m^{-1}\,\frac{\mathcal{D}_K}{v_{n+1} - v_n}\,\frac{v_{n+1} + v_n}{v_{n+1} + v_n}\,, \\ \frac{m}{\Delta t}\,(v_{n+1} - v_n) &= -\frac{V(l_{n+1}) - V(l_n) + \mathcal{D}_V}{l_{n+1} - l_n}\,\frac{q_{n+1} + q_n}{l_{n+1} + l_n}\,, \end{aligned}\right\} \tag{3.35}$$

that is, as the EDMC-1 scheme presented in this reference, but with the dissipation functions

$$\mathcal{D}_V = \tfrac{1}{2}\,\hat{K}_n(\tilde{l}_n - l_n)(l_{n+1} - l_n)\,, \quad \text{and} \quad \mathcal{D}_K = \tfrac{1}{2}\,m\,(\tilde{v}_n - v_n)(v_{n+1} - v_n)\,, \tag{3.36}$$

where $\hat{K}_n := V''(l_n) \geq 0$ (or its convexification) and, similar to (3.29),

$$\tilde{l}_n = l_n + \alpha\,\Delta t\,(\tilde{v}_n - v_{n+1})\,, \tag{3.37}$$

$$m\,\tilde{v}_n = m\,v_n - \alpha\,\Delta t\,\hat{K}_n\,(\tilde{l}_n - l_{n+1})\,, \tag{3.38}$$

with no need to introduce additional length parameters. Here, we have used the notation of $\boldsymbol{q}_t \in \mathbb{R}^2$ for the position vector at time t of the mass m from the fixed end and $\boldsymbol{v}_t \in \mathbb{R}^2$ for the velocity vector of the mass at time t, with $l_t = \|\boldsymbol{q}_t\|$ and $v_t = \|\boldsymbol{v}_t\|$. The scheme (3.35)-(3.38) exhibits the same dissipation/conservation properties as summarized in Proposition 3.1 for nonlinear elastodynamics. In particular, similar arguments show unconditional energy dissipation (the energy being $H = m\ v^2/2 + V(l)$) and conservation of the angular momentum around the center (the angular momentum being $J = m\ v\ l\ \sin\phi$ for the angle ϕ between the vectors $\boldsymbol{q}$ and $\boldsymbol{v}$), while being second-order accurate in time. We refer again to Part I of this work for details on this model problem as well as for a related simplified model of thin beams. Similar arguments apply in the construction of second-order energy-dissipative, momentum-conserving schemes for this and similar nonlinear Hamiltonian systems; details are omitted. □

4. Representative Numerical Simulations

The spectral analyses presented in Section 2.2 characterize completely the numerical properties of the new ED-1 and ED-2 schemes presented in this paper for linear elastodynamics. To evaluate the performance of the newly proposed EDMC-2 scheme for nonlinear elastodynamics, we consider in this section several representative numerical simulations that verify numerically the accuracy and dissipation/conservation properties of the new scheme shown in Section 3.2.

To this purpose, we consider the finite elastic solid depicted in Figure 4.1 in its initial configuration ($t = 0$). As seen in this figure, the solid consists of a central ring with three equally spaced blades resembling a propeller. The ring has an inner radius of 0.4, outer radius of 0.5 and depth of 0.2, and it is discretized in 15 equally spaced groups of 6 8-node bricks each. The distance from the the center of the ring to the tip of the blades is 2.5, having a twisted reference shape in between, with linearly varying thickness along its height. We have included in Figure 4.2 the coordinates of the nodes at the tip and at the base of one of the blades. A total of 12 8-node bricks are used for each blade.

The compressible Neo-Hookean model given by the stored energy function

$$W(\boldsymbol{C}) = \frac{\lambda}{2}\log^2 J + \tfrac{1}{2}\,\mu(I_1 - 3) - \mu \log J\,, \tag{4.1}$$

for $J = \sqrt{\det \boldsymbol{C}}$ and $I_1 = \operatorname{tr} \boldsymbol{C}$, and material parameters λ and μ (the Lamé constants), is considered. As indicated in the previous section, the numerical properties of the proposed schemes generalize to any elastic potential. The parameters $\lambda_b = 57.70$ and $\mu_b = 38.46$ are assumed for the blades. The inner ring is assumed stiffer, with $\lambda_r = 8 \cdot \lambda_b$ and $\mu_r = 8 \cdot \mu_b$. The reference density is taken to be $\rho_o = 8.93$ throughout.

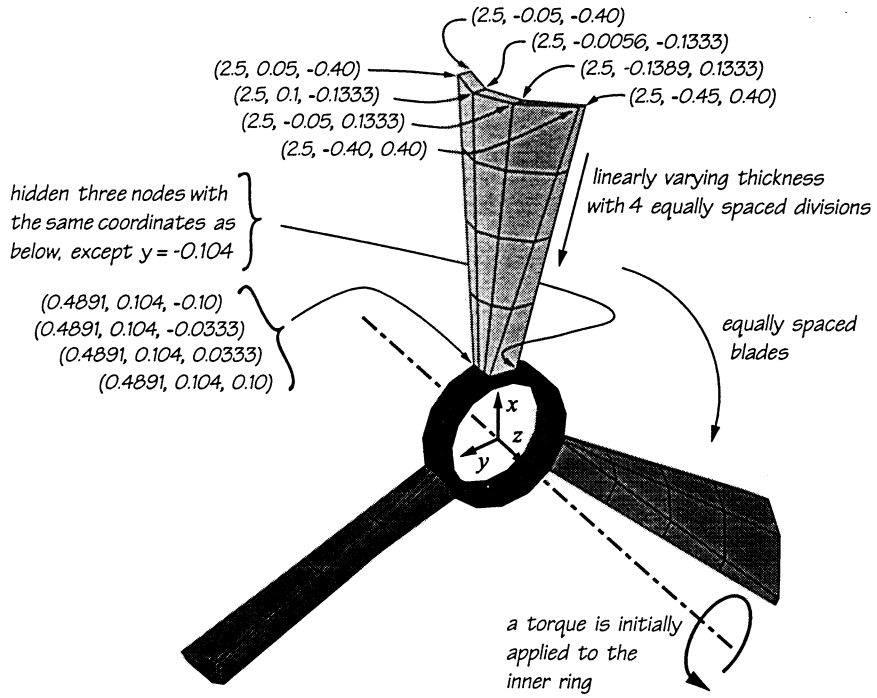

FIGURE 4.1. Three-dimensional, Neo-Hookean solid: problem definition. The solid consists of a ring of inner radius 0.4, outer radius 0.5, and depth 0.2, discretized with 90 8-node bricks. Three equally spaced blades, with a linearly varying thickness, are discretized with 12 finite elements each. The coordinates shown are given in the depicted $x - y - z$ Cartesian system, with the axis of the ring corresponding to the $z-$axis.

A volumetric body force is applied initially to the inner ring only, with the form

$$\rho_o \boldsymbol{B}(\boldsymbol{X}, t) = \tau(t) \ [\boldsymbol{e}_3 \times \boldsymbol{\varphi}(\boldsymbol{X}, t)] \ , \tag{4.2}$$

where $\boldsymbol{e}_3$ is the unit vector in the direction of the undeformed ring axis (the z-axis in Figure 4.1), and $\boldsymbol{\varphi}(\boldsymbol{X}, t)$ is the current position of the material particle $\boldsymbol{X}$. No boundary loading nor displacements are imposed. Different loading functions $\tau(t)$ are considered in the sections that follow. The mid-point approximation of the forcing term in (3.9) is considered.

With this problem at hand, we verify first in Section 4.1 the second-order accuracy of the proposed scheme. Section 4.2 focuses on the evaluation of the dissipation/conservation properties of the proposed scheme summarized in Proposition 3.1. Section 4.3 assesses in more detail the performance of the numerical schemes under study for a complex forced motion.

4.1. Evaluation of the numerical accuracy in time

We verify in this section that the theoretical second-order accuracy in time of the new EDMC-2 is actually observed in numerical simulations. A triangular loading function $\tau(t)$ in (4.2) is considered, with values

$$\tau(t) = \begin{cases} 50\dfrac{t}{7.5}\,, & 0 \le t \le 7.5\,, \\ 50\dfrac{15-t}{7.5}\,, & 7.5 \le t \le 15\,, \\ 0\,, & t \ge 15\,. \end{cases} \tag{4.3}$$

Therefore, the solid is in free motion after $t \ge 15$ ($\tau(t) = 0$ thereafter). We run the simulations for a fixed period of time $[0, 30]$, different steps sizes Δt and different values of the algorithmic parameter α.

We report in Figure 4.2 the Euclidean norm of the errors in the nodal displacements and nodal velocities, that is,

$$e_d := \left[\sum_{A=1}^{n_{node}} \|\boldsymbol{d}^A - \boldsymbol{d}^A_{lim}\|^2 \right]^{1/2} \quad \text{and} \quad e_v := \left[\sum_{A=1}^{n_{node}} \|\boldsymbol{v}^A - \boldsymbol{v}^A_{lim}\|^2 \right]^{1/2}, \tag{4.4}$$

where the "limit" solution, approximating the exact solution, is taken to be the solution computed with a very small time step ($\Delta t = 1 \cdot 10^{-3}$) and the conserving scheme ($\alpha = 0$). The results for $\alpha = 0$ (energy-momentum conserving scheme), $\alpha = 1/8$ and $\alpha = 1/6$ are depicted in this figure. The spatial discretization is kept fixed. The results presented in Figure 4.2 verify the second-order accuracy of the EDMC-2 scheme for all cases. In fact, we observe that the introduction of the numerical dissipation through the algorithmic parameter $\alpha \neq 0$ leads to numerical errors of the same order as in the conserving scheme $\alpha = 0$. Figure 4.3 depicts the final deformed configuration of the solid, computed with the EDMC-2 for $\alpha = 1/8$ and $\Delta t = 1 \cdot 10^{-2}$. The significant amount of straining of the solid is apparent.

We note that, in contrast with its linear counterpart (the ED-2 scheme of Section 2.1.2), the case $\alpha = 1/6$ does not lead to a third-order scheme in time, but second-order only. This result can be traced back to the forms of the dissipative stress and velocity terms in (3.10) and (3.15), respectively, irrespective of the order of the dissipation functions $\mathcal{D}_W$ and $\mathcal{D}_v$. Remember that the particular form employed in these expressions was motivated by the need to conserve angular momenta and corresponding relative equilibria (a feature much more important that the added extra degree of accuracy, we would say), thus leading to a numerical scheme that shows the right qualitative dynamics while still showing the desired controlled numerical dissipation in the internal modes of the motion. These dissipation/conservation properties are evaluated in the following section.

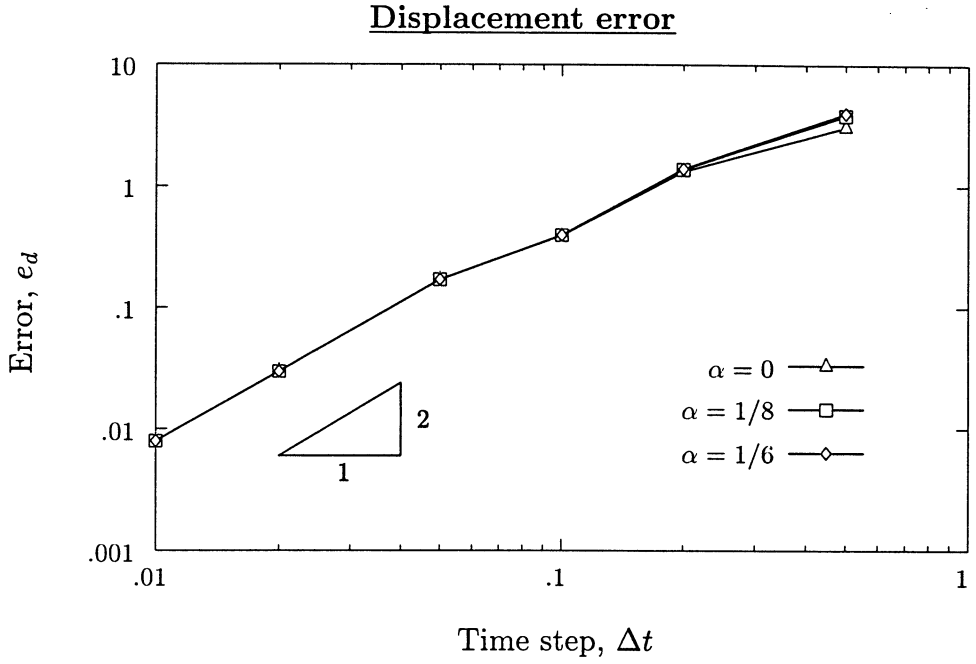

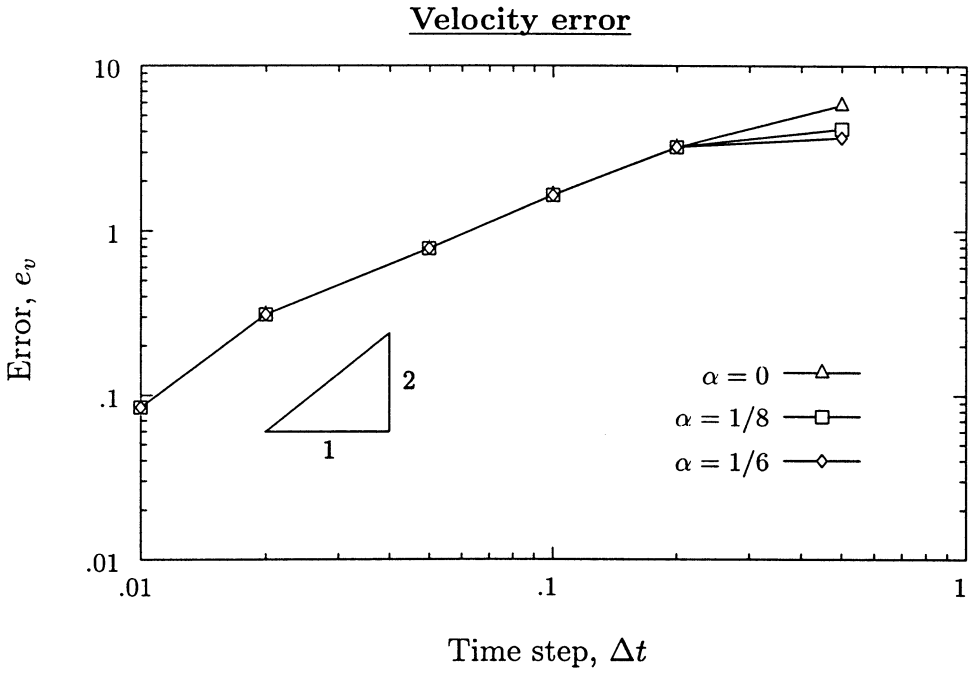

FIGURE 4.2. Three-dimensional, Neo-Hookean solid. Convergence plots for the Euclidean norm of the nodal errors of the displacements and velocities. The second-order accuracy of the EDMC-2 scheme is verified.

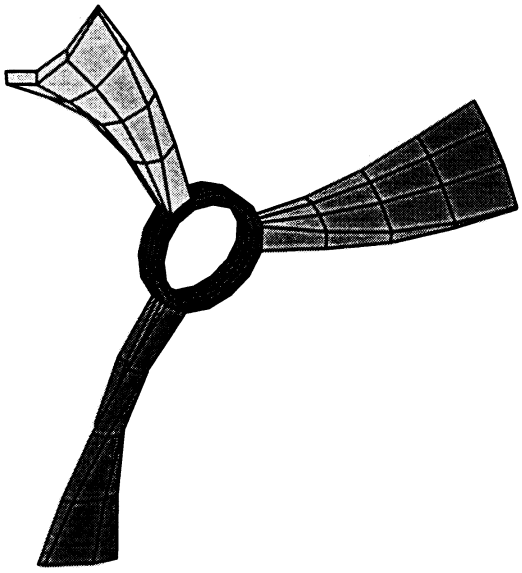

FIGURE 4.3. Three-dimensional, Neo-Hookean solid. Deformed configuration at $t = 30$, computed with the EDMC-2 scheme, with $\alpha = 1/8$ and $\Delta t = 1 \cdot 10^{-2}$.

4.2. Evaluation of the dissipation/conservation properties

To verify the dissipation/conservation properties summarized in Proportion 3.1, we compute the long-term solution of the same problem considered in the previous section under the loading function (4.3). We carry out the numerical simulation with the EDMC-2 scheme with an algorithmic parameter of $\alpha = 1/8$, and constant step-size of $\Delta t = 0.2$ for a final time of $t = 1510$.

Figure 4.4 shows the configuration of the deforming solid during the initial stages of the simulation. The varying deformation of the blades and the inner ring is apparent. In particular, we can observe the twisting and bending of the blades, characteristic of the existing high-frequency modes in the short-term solution. Figure 4.5 depicts the configuration of the solid in the final stages of the very same simulation. In particular, the absence of these high-frequency modes is apparent. In contrast, the solution is (asymptotically) closed to the relative equilibrium of the system, consisting of rigid rotation around the axis of symmetry of the solid with a fixed deformation of the blades and inner ring. No translation is involved due to the symmetry in the problem.

Figure 4.6 depicts this relative equilibrium configuration, but computed directly from the equilibrium equation for the imposed angular momentum (the angular momentum after the initial loading phase). That is, we solve the system of finite element equations

$$\int_{\mathcal{B}} N_A \, \rho_o \, [\boldsymbol{\Omega}_e \times (\boldsymbol{\Omega}_e \times \boldsymbol{\varphi}_e)] \, d\mathcal{B} + \int_{\mathcal{B}} \boldsymbol{B}_A^T \, \boldsymbol{S}(\boldsymbol{\varphi}_e) \, d\mathcal{B} = 0 \, , \quad A = 1, n_{node} \, , \tag{4.5}$$

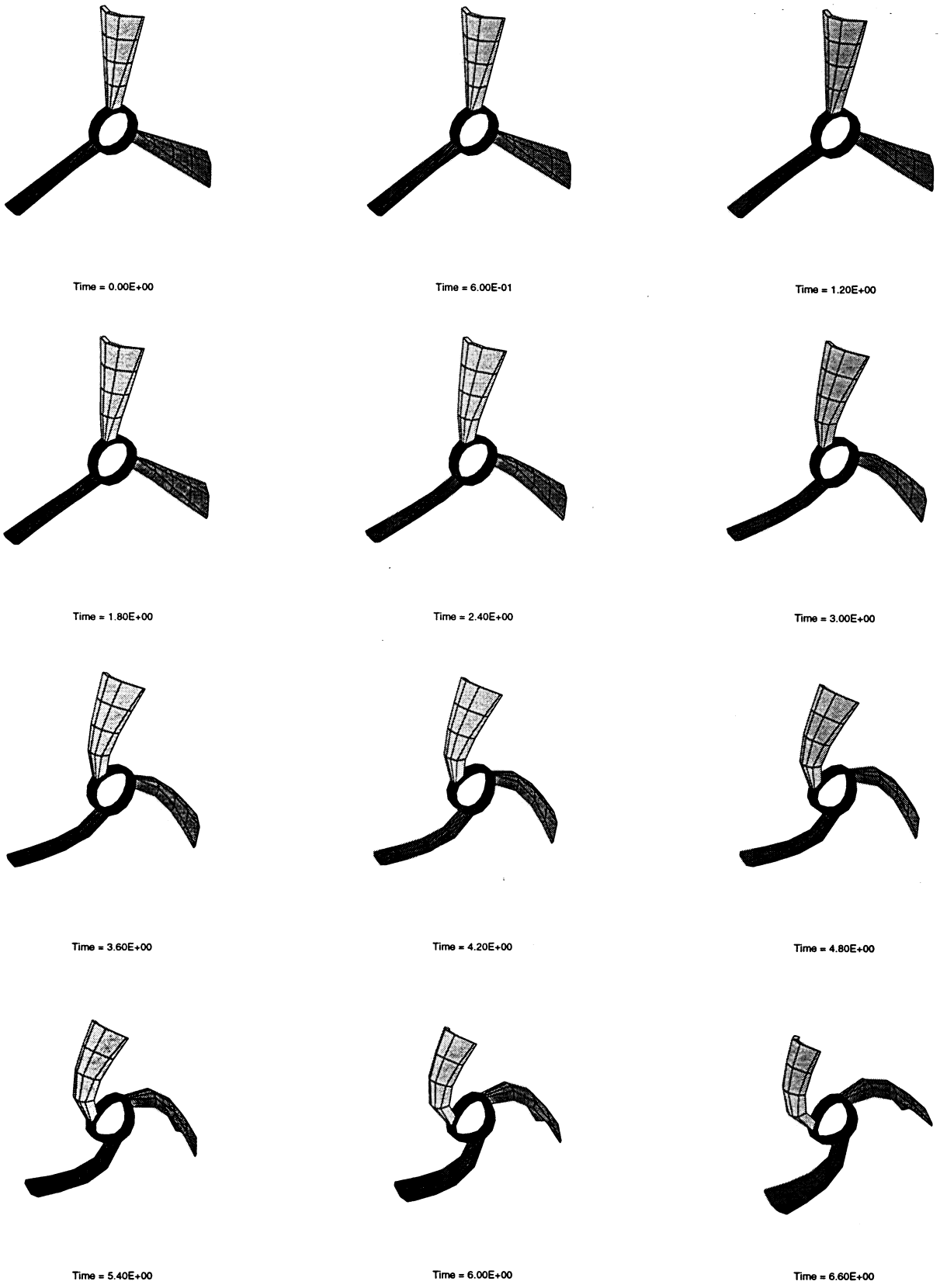

FIGURE 4.4. Three-dimensional, Neo-Hookean solid. Solution obtained with the new energy-dissipative, momentum-conserving (EDMC-2) time-stepping scheme. Initial stages (short-term solution).

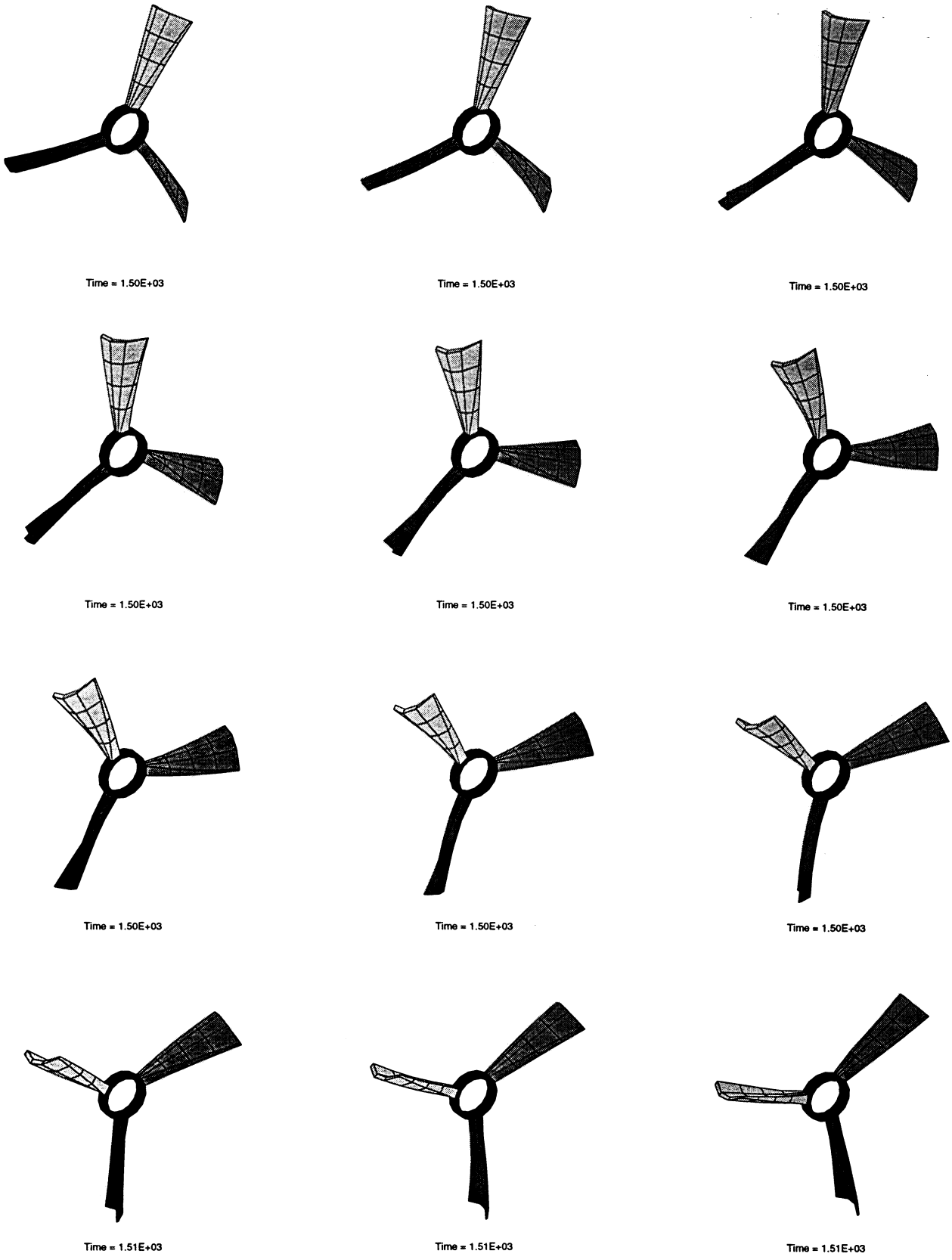

FIGURE 4.5. Three-dimensional, Neo-Hookean solid. Solution obtained with the new energy-dissipative, momentum-conserving (EDMC-2) time-stepping scheme. Final stages (long-term solution).

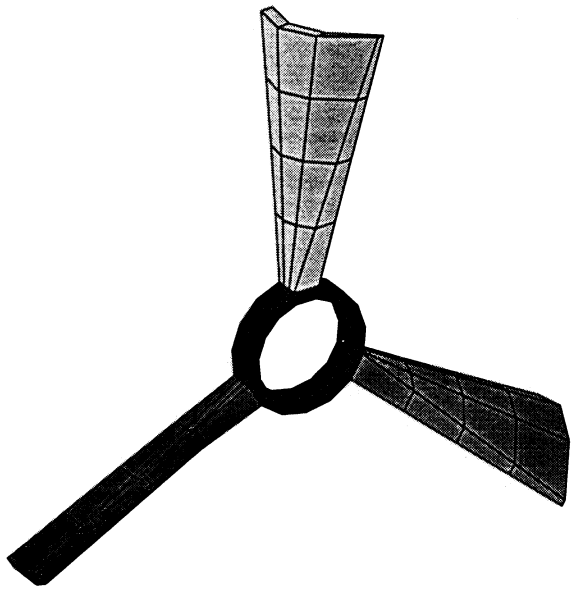

FIGURE 4.6. Three-dimensional, Neo-Hookean solid. Relative equilibrium configuration computed by solving directly the equilibrium equation (4.5).

for the equilibrium configuration φ_e. Here, the equilibrium angular velocity $\boldsymbol{\Omega}_e$ has the same axis as the imposed angular momentum $\boldsymbol{J}_e$, and it is incremented until the known value of the angular momentum $\|\boldsymbol{J}_e\|$ is obtained. We note that the equilibrium velocity field at the relative equilibrium is given by

$$\boldsymbol{v}_e = \boldsymbol{\Omega}_e \times \boldsymbol{\varphi}_e \,, \tag{4.6}$$

with the corresponding angular momentum given by the expression (3.5). The imposed boundary conditions when solving the equations (4.5) for φ_e restrict the translations along the axis defined by $\boldsymbol{\Omega}_e$ as well as the rotations around this same axis. Physically, equation (4.5) corresponds to the balance between the internal stresses at the equilibrium configuration $\boldsymbol{S}(\boldsymbol{\varphi}_e)$ and the centrifugal forces associated to the rigid rotation $-\boldsymbol{\Omega}_e \times (\boldsymbol{\Omega}_e \times \boldsymbol{\varphi}_e)$. Note that a consistent approximation has been assumed for this forcing term, as reflected by the integral involving the shape function N_A in the first term of (4.5), in accordance with the consistent approximation of the transient term assumed in the EDMC-2 scheme.

We observe that the computed long-term solution in the dynamic simulation with the newly proposed EDMC-2 agrees with this equilibrium position. Figure 4.7 includes the evolution of the three components of the angular momenta $\boldsymbol{J}^h$ and the total energy H^h (kinetic plus strain energies). After the initial loading stages, we can observe the conservation of the angular momentum and the monotonic decay of the total energy, as shown in

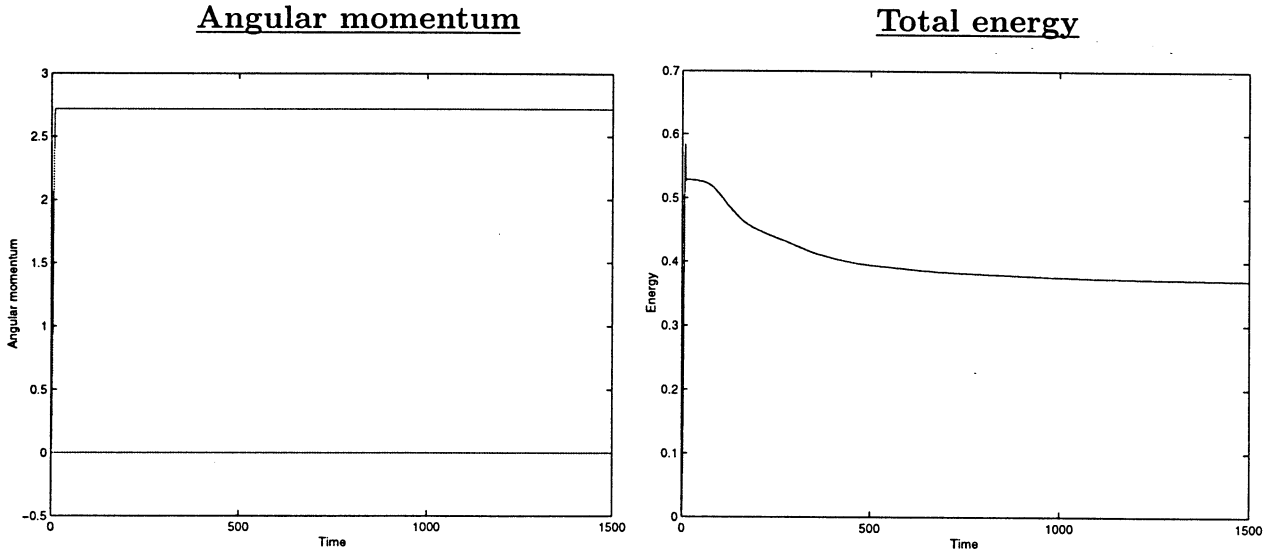

FIGURE 4.7. Three-dimensional, Neo-Hookean solid. Solution obtained with the new energy-dissipative, momentum-conserving (EDMC-2) time-stepping scheme. Evolution of the three components of the angular momentum $\boldsymbol{J}^h$ and total energy H^h.

Proposition 3.1 above. In particular, we observe that the evolution of the energy converges asymptotically to a non-zero value. In fact, to the energy of the aforementioned relative equilibrium. Moreover, further analyses show that the consideration of this equilibrium configuration with the initial velocity given by (4.6) as initial conditions leads to a numerical solution corresponding to this relative equilibrium (i.e., a rigid rotation), when computed with the proposed second-order EDMC-2 scheme. At the relative equilibrium, the EDMC-2 scheme reduces to the energy-momentum conserving scheme which leads to a second-order approximation of the equilibrium rotation, as shown in Part I of this work for general numerical schemes of the form (3.9). We refer to this reference and references therein for further details on the relative equilibria in nonlinear elastodynamics and their numerical approximation.

Therefore, we conclude that the EDMC-2 proposed in this work accomplishes then the desired high-frequency energy dissipation of the internal modes of the motion while preserving the momenta and relative equilibria of the system, and exhibiting at the same time a second-order accuracy in time. This situation is to be contrasted with the performance of traditional "dissipative" numerical schemes like the HHT α-method, as illustrated in detail in Part I of this work.

4.3. Evaluation of the numerical performance in forced motions

To conclude with the assessment of the numerical schemes under investigation, we consider in this section a problem involving a more complex forced motion. The goal is to

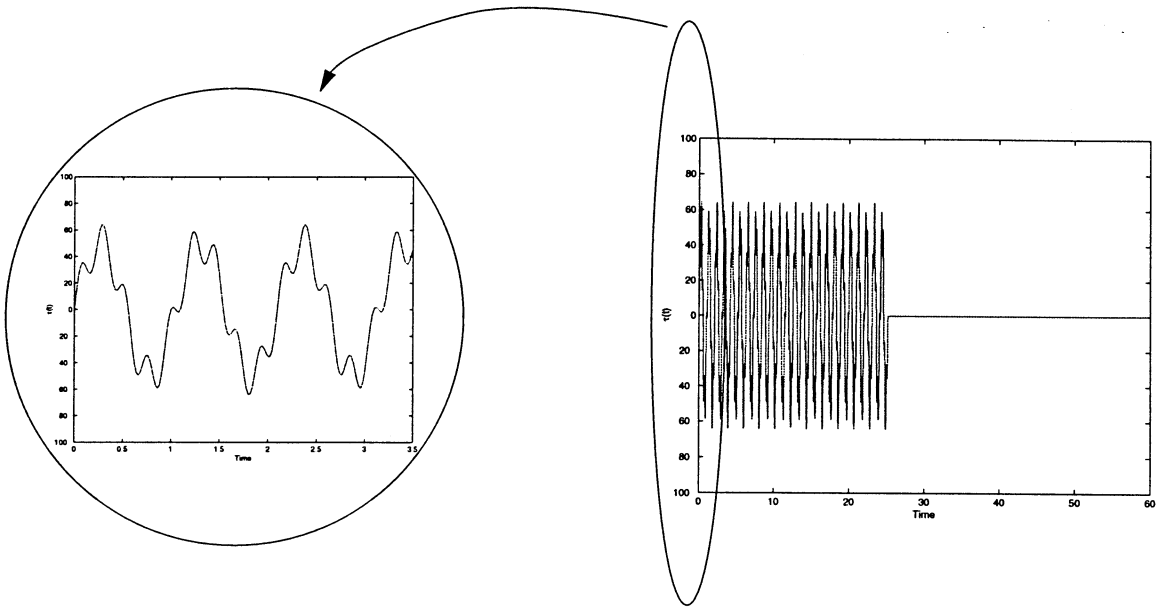

FIGURE 4.8. Three-dimensional, Neo-Hookean solid. Loading function $\tau(t) = 50\ \sin(6t) + 15\ \sin(27t)$ with $\Delta t = 0.02$.

evaluate the numerical performance of the schemes when different frequencies are excited in an extended period of time. To this purpose, we consider the same solid as employed in the previous sections, subjected to same torque distribution (4.2), but with the loading function

$$\tau(t) = \begin{cases} 50\ \sin(6t) + 15\ \sin(27t) & \text{for } t \leq 8\pi\ , \\ 0 & \text{for } t > 8\pi\ , \end{cases} \tag{4.7}$$

consisting of two sine functions with angular frequencies of 6 and 27, respectively. The solid is then released at the time $t \approx 25$. A constant time step of $\Delta t = 0.02$ is considered, resolving correctly the function $\tau(t)$ in (4.7). This function has been depicted in Figure 4.8. This specific loading has been chosen after carrying out a modal analysis of the solid in the initial undeformed configuration, consisting of a total of 828 modes. The lowest natural frequency in this configuration is $w_1 = 0.3$ with the 26^{th} natural frequency being $w_{26} = 6.0$ and the 98^{th} frequency being $w_{98} = 27.0$. A cluster of modes can also be observed around the latter value, with a total of 12 modes in the frequency range $[26.0, 28.0]$. Obviously the natural frequencies associated with the linearized problem change in time given the general large deformation framework considered herein.

Figure 4.9 (top row) depicts the solution obtained with the conserving scheme $\alpha = 0$. We have included the evolution of the total energy of the solid and the quantity

$$\|\boldsymbol{a}^h\| := \left[\int_{\mathcal{B}} \left\| \frac{\boldsymbol{v}_{n+1} - \boldsymbol{v}_n}{\Delta t} \right\|^2 d\mathcal{B} \right]^{1/2} , \tag{4.8}$$

approximating the L_2-norm of the acceleration field. The high-frequency content of the solution is apparent in the acceleration plot, which is observed to increase in time. This increase is observed not only during the period of time $[0, 8\pi]$ of application of the external force, but also after the solid is released. Even though the energy is conserved after this instant, no convergence is obtained for this step size at time $t \approx 39$. This example illustrates the lack of control on the acceleration by conserving schemes, leading to the observed difficulties in resolving motions with a high-frequency content. Additional examples involving simpler Hamiltonian systems can be found in Part I of this work.

Figure 4.9 depicts also the solutions obtained by different EDMC-2 dissipative schemes. The two values of $\alpha = 1/8$ and $1/4$ are considered. In contrast with the previous conserving scheme, the numerical acceleration can be observed to be under control, at the price of a dissipated energy upon release. No lack of convergence has been observed in these cases for this time step. The total energy and the acceleration norm (4.8) is depicted versus time for the different values of the algorithmic parameter α. The comparison of these solutions illustrates the role of this algorithmic parameter in the control of the performance (the numerical dissipation, in particular) of the numerical scheme. The presence of this parameter allows then to obtain the numerical solution in the complex motions where conserving schemes show clear difficulties in the resolution of all the components of the motion. We note that the one-step nature of the proposed scheme allows for the perfect control of the numerical dissipation introduced in the simulations by adapting the value of this algorithmic parameter, if desired, while maintaining a reasonable time step based only on accuracy considerations.

5. Concluding Remarks

We have presented in this paper a new second-order time-stepping algorithm for nonlinear elastodynamics (the EDMC-2 scheme) that exhibits rigorously the energy dissipation properties needed for the solution of stiff problems of interest, while preserving the conservation laws of linear and angular momenta and as well as the associated relative equilibria. The spectral properties of the new schemes have also been studied in detail for the system of linear elastodynamics. The ideas presented here lead to new numerical schemes even in this linear range, being second-order in time and exhibiting controlled energy dissipation in the high-frequency range. In fact, the new second-order scheme ED-2 has been shown to be L-stable, extending in this way some existing multi-stage (Runge-Kutta type) schemes.

As discussed and shown rigorously in Part I of this work, traditional "dissipative" numerical schemes, like the HHT $\alpha-$method, not only loose this dissipativity property in the nonlinear range (exhibiting numerical instabilities in the form of an uncontrollable energy growth in time), but they do not preserve either other features of the phase dynamics like relative equilibria. In contrast, the newly proposed EDMC schemes (the first-order

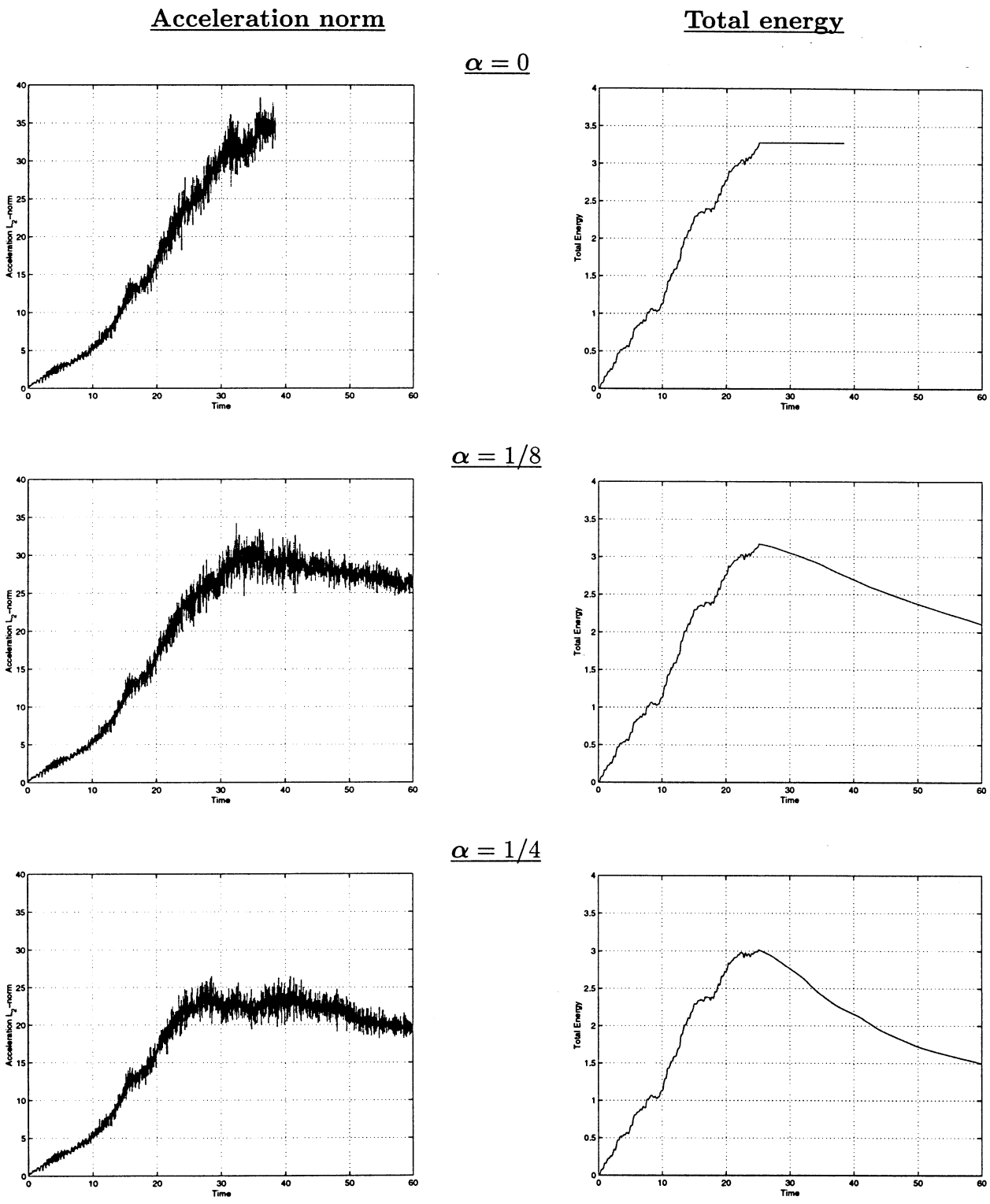

FIGURE 4.9. Three-dimensional, Neo-Hookean solid. Evolution of the total energy H^h and the L_2-norm of the numerical acceleration during forced motion, obtained with the new energy-dissipative, momentum-conserving (EDMC-2) time-stepping scheme for $\alpha = 0$ (conserving), 1/8 and 1/4.

EDMC-1 or the second-order EDMC-2) show these dissipation properties at the internal modes of the motion, as illustrated in the example of Section 4.2. We emphasize the controlled character of the numerical dissipation introduced in the numerical simulation. In particular, this numerical dissipation may be turned off at any time, if desired, while keeping it when difficulties appear with conserving approximations of the problem, as illustrated in the example presented in Section 4.3, following the standard philosophy for the use of dissipative schemes in the linear range. The limit situation presented in Section 4.2 of obtaining asymptotically the relative equilibrium illustrates the long-term properties of the proposed numerical scheme and the nature of the introduced numerical dissipation, even though we may not be interested in damping all the internal modes of the motion in particular applications. On the other hand, the proposed schemes appear as an efficient tool for obtaining these equilibrium solutions.

In this respect, and based on our experience, we find fundamental that the numerical scheme preserves the conservation law of angular momentum at all times, an intrinsically nonlinear property as indicated in the introduction, and hence absent in standard high-frequency "dissipative" schemes. The need to assure this property leads necessarily to complex nonlinear formulae when compared, for example, to the ideas presented herein for the linear range. Nonetheless, the construction of the energy dissipative properties in nonlinear elastodynamics has been shown in this paper to follow the same arguments presented for the linear problem, but at the level of the quadrature points of a typical finite element implementation of these methods. This strategy avoids the additional large computational cost associated with the doubling of the number of unknowns in each time step for each stage of a globally defined multi-stage formula (typical, for example, of discontinuous Galerkin-type approaches), with a fully coupled algebraic system of equations between all these stages. Still, the new scheme requires the coupled solution for the nodal displacements and velocities of the single stage, as described in detail in Appendix I. We presented in Part I of this work how a lumped implementation of these ideas led to a more standard implementation for the first-order EDMC-1 scheme, involving the solution of an algebraic system of equations for the nodal displacements combined with independent (nonlinear) nodal updates. The development of efficient strategies for the solution of the extended systems associated to the second-order EDMC-2 scheme proposed herein is one of the focus of our current work. Similarly, the ideas presented in this paper can be applied to time-stepping algorithms in the rotation group, with applications in the stable integration of geometrically exact rod and shell theories, as we plan to present in a forthcoming publication.

Acknowledgments: Financial support for this research was provided by the AFOSR under contract no. F49620-97-1-0196 with UC Berkeley. This support is gratefully acknowledged.

References

ARMERO, F. & PETOCZ, E. [1996] "Formulation and Analysis of Conserving Algorithms for Fricitonless Dynamic Contact/Impact Problems," *Comp. Meth. Appl. Mech. Engr.*, **158**, 269-300.

ARMERO, F. & ROMERO, I. [1999] "On the Formulation of High-Frequency Dissipative Time-Stepping Algorithms for Nonlinear Dynamics, Part I: Low Order Methods for Two Model Problems and Nonlinear Elastodynamics," UCB/SEMM Rep. 99-05 (submitted to *Comp. Meth. App. Mech. Eng.*)

BAUCHAU, O.A., DAMILANO, G. & THERON, N.J. [1995] "Numerical Integration of Nonlinear Elastic Multi-Body Systems," *Int. J. Num. Meth. Eng.*, **38**, 2727-2751.

BAUCHAU, O.A. & THERON, N.J. [1996] "Energy Decaying Scheme for Non-linear Beam Models," *Comp. Meth. Appl. Mech. Engr.*, **134**, 37-56.

BAUCHAU, O.A. & JOO, T. [1999] "Computational Schemes for Non-linear Elasto-Dynamics," *Int. J. Num. Meth. Eng.*, **45**, 693-719.

BOTASSO, C. & BORRI, M. [1998] "Integrating Rotations," *Comp. Meth. Appl. Mech. Engr.*, **164**, 307-331.

CRISFIELD, M.A.; GALVANETTO, U. & JELENIC, G. [1997] "Dynamics of 3-D Co-Rotational Beams," *Computational Mechanics*, **20**, 507-519.

CRISFIELD, M. & SHI, J. [1994] "A Co-Rotational Element/Time-Integration Strategy for Non-Linear Dynamics," *Int. J. Num. Meth. Eng.*, **37**, 1897-1913.

DACOROGNA, B. [1989] *Direct Methods in the Calculus of Variations*, Springer-Verlag, New York.

GONZALEZ, O. & SIMO, J.C. [1996] "On the Stability of Symplectic and Energy-Momentum Algorithms for Nonlinear Hamiltonian Systems with Symmetry," *Comp. Meth. Appl. Mech. Eng.*, **134**, p 197-222.

GONZALEZ, O. & J.C. SIMO [1995] "Exact Energy-Momentum Conserving Algorithms for General Models in Nonlinear Elasticity," *Comp. Meth Appl. Mech. Eng.*, to appear.

HAIRER, E. & WANNER, G. [1991] *Solving Ordinary Differential Equations II: Stiff and Differential-Algebraic Problems*, Springer-Verlag, Berlin.

HILBER, H.M; HUGHES, T.J.R.; TAYLOR, R.L. [1977] "Improved numerical dissipation for time integration algorithms in structural dynamics", *Earthquake engineering and Structural Dynamics* **5**, 283-292.

HUGHES, T.J.R. [1987] *The Finite Element Method,* Prentice-Hall,

HUGHES, T.J.R. [1983] "Analysis of transient algorithms with particular reference to stability behaviour," *Computational methods for transient analysis, Ed. T. Belytschko, T.J.R. Hughes, North-Holland*

HUGHES, T.J.R. & HULBERT, M. [1988] "Space-time Finite Element Methods for Elastodynamics: Formulation and Error Estimates," *Comp. Meth. App. Mech. Engr.* **66**, 339-363.

JOHNSON, C.; NÄVERT, U. & PITKÄRANTA, J. [1984] "Finite Element Methods for Linear Hyperbolic Problems," *Comp. Meth. App. Mech. Engr.,* **45**, 285-312.

KUHL, D. & CRISFIELD, M.A. [1997] "Energy Conserving and Decaying Algorithms in Non-Linear Structural Dynamics", *Int. J. Num. Meth. Eng.,* **45**, 569-599.

KUHL, D. & RAMM, E. [1996] "Constraint Energy Momentum Algorithm and its Application to Non-Linear Dynamics of Shells," *Comp. Meth. App. Mech. Engr.,* **136**, 293-315.

KUHL, D. & RAMM, E. [1999] "Generalized Energy-Momentum Method for Non-linear Adaptive Shell Dynamics," *Comp. Meth. App. Mech. Engr.,* **178**, 343-366.

MARSDEN, J.E. [1992] *Lectures on Mechanics,* London Mathematical Society Lecture Note Series, **174**, Cambridge University Press.

NEWMARK, N.M. [1959] "A Method of Computation for Structural Dynamics," *Journal of the Engineering Mechanics Division ASCE,* 67-94.

SIMO, J.C. & GONZALEZ, O. [1994] "Recent Results on the Numerical Integration of Infinite-Dimensional Hamiltonian Systems," in *Recent Developments in Finite Element Analysis,* ed. by T.J.R. Hughes, O. Oñate, and O.C. Zienkiewicz, CIMNE, Barcelona.

SIMO, J.C. & TARNOW, N. [1992] "The Discrete Energy–Momentum Method. Conserving Algorithms for Nonlinear Elastodynamics," *ZAMP,* **43**, 757-793.

WOOD, W.L. [1990] *Practical Time-Stepping Schemes,* Clarendon Press, Oxford.

Appendix I. Implementation of the EDMC-2 scheme

We summarize in this appendix the numerical implementation of the newly proposed second-order energy-dissipative, momentum-conserving EDMC-2 scheme. We begin by writing the discrete finite element equations (3.9) in the following residual form

$$\boldsymbol{R}(\boldsymbol{d}_{n+1}, \boldsymbol{v}_{n+1}) = \left\{ \begin{array}{c} \boldsymbol{R}^1 \\ \boldsymbol{R}^2 \\ \vdots \\ \boldsymbol{R}^{n_{node}} \end{array} \right\} \quad \text{with} \quad \boldsymbol{R}^A = \left\{ \begin{array}{c} \boldsymbol{R}^A_d \\ \boldsymbol{R}^A_v \end{array} \right\}, \quad A = 1, n_{node} \tag{I.1}$$

where the nodal residuals are given

$$\left. \begin{aligned} \boldsymbol{R}^A_d &= \tilde{\boldsymbol{f}}^A_{ext} - \int_{\mathcal{B}} \rho_o \, N_A \, \frac{\boldsymbol{v}_{n+1} - \boldsymbol{v}_n}{\Delta t} \, d\mathcal{B} - \int_{\mathcal{B}} \boldsymbol{B}^{A^T}_{n+\frac{1}{2}} \boldsymbol{S} \, d\mathcal{B} \\ \boldsymbol{R}^A_v &= \int_{\mathcal{B}} \rho_o \, N_A \left(\frac{\boldsymbol{d}_{n+1} - \boldsymbol{d}_n}{\Delta t} - (1 + g_{diss}) \, \boldsymbol{v}_{n+\frac{1}{2}} \right) d\mathcal{B} \end{aligned} \right\} \tag{I.2}$$

for each node $A = 1, n_{node}$. Here, the stress tensor $\boldsymbol{S}$ is given by (3.10), which can be written for the EDMC-2 scheme of interest as

$$\boldsymbol{S} = \boldsymbol{S}_{cons} + f_{diss} \, \boldsymbol{N} \,, \quad \text{for} \quad f_{diss} = \hat{\kappa} \, \tilde{\beta}_n \| \boldsymbol{C}_{n+1} - \boldsymbol{C}_n \| \,, \tag{I.3}$$

with $\boldsymbol{S}_{cons}$ given by (3.11) and (3.15), $\boldsymbol{N}$ by (3.10), $\tilde{\beta}_n$ by $(3.29)_1$ and $\hat{\kappa}$ by $(3.30)_2$. The scalar g_{diss} in $(I.2)_2$ denotes the combination

$$g_{diss} = \frac{\tilde{v}_n - v_n}{v_{n+1} + v_n} \,, \tag{I.4}$$

for $\tilde{v}_n$ given by $(3.29)_2$, $v_n = \|\boldsymbol{v}_n\|$ and $v_{n+1} = \|\boldsymbol{v}_{n+1}\|$. The integrals in (I.2), and similar ones appearing below, are computed through the standard assembly of element contributions computed through a quadrature rule.

The nonlinear system of equations $\boldsymbol{R} = 0$ is solved iteratively through a Newton scheme, leading to the algebraic system of equations

$$\boldsymbol{K}^{(k)}_{n+1} \left\{ \begin{array}{c} \delta \boldsymbol{d}^{(k)}_{n+1} \\ \delta \boldsymbol{v}^{(k)}_{n+1} \end{array} \right\} = \boldsymbol{R}(\boldsymbol{d}^k_{n+1}, \boldsymbol{v}^k_{n+1}) \,, \tag{I.5}$$

with $\boldsymbol{d}^{(k+1)} = \boldsymbol{d}^{(k)}_{n+1} + \delta \boldsymbol{d}^{(k)}_{n+1}$ and $\boldsymbol{v}^{(k+1)} = \boldsymbol{v}^{(k)}_{n+1} + \delta \boldsymbol{v}^{(k)}_{n+1}$. The tangent matrix $\boldsymbol{K}^{(k)}_{n+1}$ is computed as a function of the nodal vectors $\boldsymbol{d}^{(k)}_{n+1}$ and $\boldsymbol{v}^{(k)}_{n+1}$ through the standard finite element assembly of element contributions, each contribution consisting of block

components $\boldsymbol{K}^{AB}$ for nodes A and B (the indices (k) and $n+1$ have been dropped to ease the notation). We can write

$$\boldsymbol{K}^{AB} = \begin{bmatrix} \boldsymbol{K}^{AB}_{dd} & \boldsymbol{K}^{AB}_{dd} \\ \boldsymbol{K}^{AB}_{vd} & \boldsymbol{K}^{AB}_{vv} \end{bmatrix} , \tag{I.6}$$

with each sub-block being the square $n_{\text{dim}} \times n_{\text{dim}}$ matrices

$$\boldsymbol{K}^{AB}_{dd} = \int_{\mathcal{B}} \boldsymbol{B}^{A^T}_{n+\frac{1}{2}} \, \mathbb{C}_{cons} \, \boldsymbol{B}^{B}_{n+1} \, d\mathcal{B} + \int_{\mathcal{B}} \boldsymbol{B}^{A^T}_{n+\frac{1}{2}} \, \mathbb{C}_{diss} \, \boldsymbol{B}^{B}_{n+1} \, d\mathcal{B} + \int_{\mathcal{B}} \tfrac{1}{2} G_{AB} \, \mathbf{1} \, d\mathcal{B} \, , \tag{I.7}$$

$$\boldsymbol{K}^{AB}_{dv} = \frac{1}{\Delta t} M_{AB} \, \mathbf{1} + \int_{\mathcal{B}} \boldsymbol{B}^{A^T}_{n+\frac{1}{2}} \, \boldsymbol{D} \, d\mathcal{B} \, , \tag{I.8}$$

$$\boldsymbol{K}^{AB}_{vd} = \frac{1}{\Delta t} M_{AB} \, \mathbf{1} + \int_{\mathcal{B}} \rho_o \, \gamma_6 \, N_A \, \boldsymbol{v}_{n+\frac{1}{2}} \, \tilde{\boldsymbol{N}}^T \, \boldsymbol{B}^{B}_{n+1} \, d\mathcal{B} \, , \tag{I.9}$$

$$\boldsymbol{K}^{AB}_{vv} = \tfrac{1}{2} M_{AB} \, \mathbf{1} + \int_{\mathcal{B}} \gamma_5 \, N_A \, N_B \, \boldsymbol{v}_{n+\frac{1}{2}} \otimes \frac{\boldsymbol{v}_{n+1}}{v_{n+1}} \, d\mathcal{B} \, , \tag{I.10}$$

where the scalar M_{AB} is given by $(3.8)_2$ and we have introduced the notation

$$\begin{aligned} \mathbb{C}_{cons} = {} & \frac{1}{\nu} \boldsymbol{N} \otimes \boldsymbol{S}_{n+1} + \frac{2}{\nu} \left[\boldsymbol{N} \cdot \partial_C W(\frac{\boldsymbol{C}_{n+1} + \boldsymbol{C}_n}{2}) - \frac{W(\boldsymbol{C}_{n+1}) - W(\boldsymbol{C}_n)}{\nu} \right] \boldsymbol{N} \otimes \boldsymbol{N} \\ & - \frac{1}{\nu} \left[\boldsymbol{N} \cdot \partial_C W(\frac{\boldsymbol{C}_{n+1} + \boldsymbol{C}_n}{2}) - \frac{W(\boldsymbol{C}_{n+1}) - W(\boldsymbol{C}_n)}{\nu} \right] \mathbb{I} - \frac{1}{\nu} \boldsymbol{N} \otimes \partial_C W(\frac{\boldsymbol{C}_{n+1} + \boldsymbol{C}_n}{2}) \\ & + 2 \, \partial^2_{CC} W(\frac{\boldsymbol{C}_{n+1} + \boldsymbol{C}_n}{2}) - \boldsymbol{N} \otimes \left(2 \, \partial^2_{CC} W(\frac{\boldsymbol{C}_{n+1} + \boldsymbol{C}_n}{2}) \boldsymbol{N} \right) , \end{aligned} \tag{I.11}$$

$$\mathbb{C}_{diss} = \tfrac{1}{2} \, \hat{\kappa} \, \nu \, \gamma_1 \, \boldsymbol{N} \otimes \boldsymbol{N} + \tfrac{1}{2} \, \hat{\kappa} \, \tilde{\beta}_n \mathbb{I} \, , \tag{I.12}$$

$$G_{AB} = \sum_{I,J=1}^{n_{\text{dim}}} \frac{\partial N_A}{\partial X^I} \, S_{IJ} \, \frac{\partial N_B}{\partial X^J} \, , \qquad \boldsymbol{D} = \tfrac{1}{2} \, \gamma_2 \, \boldsymbol{N} \otimes \boldsymbol{v}_{n+1} \, , \tag{I.13}$$

$$\tilde{\boldsymbol{N}} = (N_{11}, N_{22}, N_{33}, N_{12}, N_{23}, N_{13})^T \, , \tag{I.14}$$

$$\gamma_1 = \frac{2 \, \alpha^2 \, c^2 \, \Delta t^2 \, \nu \, (1 - \tilde{\beta})}{\tilde{\Delta}} \, , \qquad \gamma_2 = \frac{\alpha \, \Delta t \, h \, \nu \, \hat{\kappa}}{\tilde{\Delta} \, v_{n+1}} \, , \tag{I.15}$$

$$\gamma_3 = 1 - \frac{h^2}{\tilde{\Delta}} \, , \qquad \gamma_4 = -\frac{2 \, \alpha \, c^2 \, \Delta t \, \nu}{\tilde{\Delta}} (h + \alpha \, \Delta t (\tilde{v}_n - v_{n+1})) \, , \tag{I.16}$$

$$\gamma_5 = \frac{\gamma_3 - g_{diss}}{v_n + v_{n+1}} , \qquad \gamma_6 = \frac{\gamma_4}{v_{n+1} + v_n} , \tag{I.17}$$

$$\nu = 2\|\boldsymbol{C}_{n+1} - \boldsymbol{C}_n\| , \qquad \tilde{\Delta} = h^2 + \alpha\, c^2\, \Delta t^2\, \nu^2 , \tag{I.18}$$

which simplify for the limit case $\|\boldsymbol{C}_{n+1} - \boldsymbol{C}_n\| \to 0$ to the values $\mathbb{C}_{cons} = 2\,\partial^2_{CC} W((\boldsymbol{C}_{n+1} + \boldsymbol{C}_n)/2)$, $\mathbb{C}_{diss} = 0$ and $\boldsymbol{D} = 0$. The values h and c in these expressions are defined in (3.30).